Evaluating adipose stromal cell tenogenic differentiation on micropatterned polyurethane 3D printed scaffolds

Submitted by

GARGI GOEL

3D Bioprinting Lab and Regenerative Orthopaedics and Innovation Laboratory

Experimental Surgery, Faculty of Medicine and Health Sciences

McGill University

Montreal, Quebec, Canada

A thesis submitted to McGill University in partial fulfillment of the requirements of the degree of Master of Science (M.Sc.)

© Gargi Goel, August 2022

TABLE OF CONTENTS

ABSTRACT

Anterior cruciate ligament (ACL) injuries are common musculoskeletal traumas, leading to knee instability and reduced knee function. Due to the insufficient self-healing capacity of ACL, surgical reconstruction with tendon allograft or autograft is often required. But it fails to restore its biomechanical functions to pre-injury activity levels, leading to re-injury. ACL tissue engineering applications aim to repair and regenerate the ligament/tendon tissue by generating a cell-seeded scaffold that can mimic the anisotropic architecture of the native tissue, thereby producing a graft substitute which can restore pre-injury activity levels with reduced risks of postoperative complications and graft failures. A current challenge to this approach is to generate a scaffold with biomechanical properties comparable to the ACL and find a cell source that can lay down native ACL tissue matrix on the scaffold, resulting in better integration of the bioengineered implant. Thus, in this study, we generated low-cost 3D-printed bioscaffolds using thermoplastic elastomeric material, i.e., LayFOMM60 and Layfelt, and determined its mechanical, chemical, and biological properties for further development as implantable ACL tissue substitutes. Furthermore, we investigated the potential of adipose stromal cells to act as a potential cell source for ligamentogenesis/tenogenesis and its compatibility with LayFOMM60 and Layfelt. Results suggest that LayFOMM60 and Layfelt are biocompatible and promote tenogenic/ligamentogenic differentiation of adipose stromal cells by ligament/tendon matrix deposition.

RESUME

Les lésions du ligament croisé antérieur (LCA) sont fréquentes, entraînant une instabilité du genou et une réduction de la fonction du genou. En raison de la faible capacité d'auto-guérison du LCA, une reconstruction chirurgicale avec autogreffe de tendon est souvent nécessaire, mais elle ne parvient pas à restaurer ses fonctions biomécaniques à des niveaux d'activité préopératoire, ce qui peut entraîner une nouvelle blessure. L'ingénierie tissulaire vise à réparer et à régénérer le tissu ligamentaire/tendineux en générant un échafaudage ensemencé de cellules qui peut imiter l'architecture anisotrope du tissu natif, produisant ainsi un substitut de greffe qui peut restaurer les niveaux d'activité avant la blessure, avec des risques réduits de complications postopératoires. Un défi actuel de cette approche est de former un échafaudage qui a des propriétés biomécaniques comparables au LCA et de trouver une source cellulaire qui peut régénérer le tissu conjonctif perdu, résultant en une meilleure intégration de l'implant. Ainsi, dans cette étude, nous avons généré des échafaudages imprimés en 3D à faible coût en utilisant un matériau élastomère thermoplastique, c'est-à-dire LayFOMM60 et Layfelt, et déterminé ses propriétés mécaniques, chimiques et biologiques pour le développement d'implant de substitut de tissu LCA. De plus, nous avons étudié le potentiel des cellules stromales adipeuses à agir comme source cellulaire pour la ligamentogenèse/ténogenèse et sa compatibilité avec LayFOMM60 et Layfelt. Les résultats suggèrent que LayFOMM60 et Layfelt sont biocompatibles et favorisent la différenciation ténogène/ligamentogène des cellules stromales adipeuses par dépôt de matrice ligament/tendon.

ACKNOWLEDGEMENTS

I am tremendously grateful to my supervisors, Dr. Derek H. Rosenzweig and Dr. Rahul Gawri, for their extensive knowledge, invaluable advice, unwavering patience, and tutelage. Derek, for your encouragement and unparalleled support, and Rahul, for your practical suggestions and profound belief in me. I am thankful to my research advisory committee, Dr. Ahmed Aoude, Dr. Paul Martineau, and Dr. Chan Gao, for their time and feedback. Special gratitude to Dr. Paul Martineau, Dr. Joshua Vorstenbosch, Dr. Suliman Mohammed Alshammari, and Dr. Hillary Nepon for providing me with ACL and adipose tissue samples, without which my research would not have been possible. I appreciate Dr. Sophie Lerouge, Dr. Julie Fradette and Atma Adoungotchodo for their expertise and valuable insight into the project and ThéCell for funding this research project.

I am immensely thankful to all my lab members and fellow researchers for their support and friendship. While sharing laughs and overcoming hurdles together, you guys have been like a family to me. To Ateeque Siddique, from helping in logistics, and providing valuable feedback, to hearing me out, you have been an incredible friend. To Hyeree Park, Megan Cooke and Jean Gabriel Lacombe for helping me plan and develop the research work. To Audrey Pitaru, Eleane Hamburger, Paraskevi Tselekouni, Laura Bouret, Mansoureh Mohseni, Neda Azizipour, Li Li, Cameliya Sinha Roy, Rayan Ben Letaifa, Prabhu Karthick Parmeshwar and Cedric Julien for your assistance and friendship.

I extend my deepest gratitude towards my parents, my brothers Vaibhav Goel and Abhishek Goyal. To all my friends and teachers for supporting me and advising me through all thick and thins.

LIST OF FIGURES

LIST OF TABLES

ABBREVIATIONS

AA	Antibiotic-antimycotic
ACL	Anterior cruciate ligament
AM	Antero-medial
ASCs	Adipose stromal cells
CAD	Computer-aided design
DI	Distilled water
DIEP	Deep inferior epigastric perforator
DMEM	Dulbecco's modified Eagle standard growth medium
DNA	Deoxyribonucleic acid
ECM	Extra cellular matrix
ESCs	Embryonic stem cells
EDTA	Ethylenediaminetetraacetic acid
FBS	Fetal bovine serum
FDM	Fused deposition modelling
HGF	Hepatocyte growth factor
iPSCs	Induced pluripotent stem cells
IGF	Insulin-like growth factor
LCL	Lateral collateral ligament
MCL	Medial collateral ligament
MRI	Magnetic resonance imaging
MSCs	Mesenchymal stem cells

PBS	Phosphate buffer saline
2X AA-PBS	2% AA in Ca^{2+}/ Mg^{2+} free PBS
PCL	Posterior cruciate ligament
PCR	Polymerase chain reaction
PDGF	Platelet derived growth factor
PGA	Polyglycolide
PL	Postero-lateral
PLA	Polylactic acid
PLGA	Polylactic co-glycoside
PVA	Polyvinyl alcohol
REB	Research ethics boards
RNA	Ribonucleic acid
RT-qPCR	Reverse transcriptase quantitative polymerase chain reaction
SCX	Scleraxis
SD	Standard deviation
T/L	Tendon and ligament
TGF	Transforming growth factor
TNC	Tenascin C
TNMD	Tenomodulin
UTS	Ultimate tensile strength
UV	Ultraviolet light
VEGF	Vascular endothelial growth factor
VSF	Vascular stromal fraction

CHAPTER 1

INTRODUCTION

Tendon and ligament injuries are among the most common injuries in the body, accounting for over 50% of musculoskeletal injuries. This poses a significant financial and healthcare burden worldwide [1, 2]. Each year, around 17 million ligamentous injuries require medical attention in the United States alone, with an associated financial burden of 40 billion USD [2]. It can range from common sprains and strains to complete tissue tears. Along with the high economic burden, these injuries significantly compromise a patient's quality of life [2] as, the primary function of these tissues is to provide stability and transfer of loads. Therefore, their injury results in a loss of function [1]. Poor vascularization and regeneration capacity of these connective tissues warrant the need for surgical intervention for their repair [3]. Tendon and ligament injuries often require surgical reconstruction using grafts. Current clinical practices rely on tendon or ligament tissue replacement using autografts or allografts [4]. The anterior cruciate ligament is one such ligament that is frequently injured in the elderly and athletes, leading to joint instability, pain, and degenerative disorders [5]. The patellar tendon, hamstring tendon and cadaveric allografts are the mainstay graft substitutes for ACL tears. Despite successful short-term outcomes, these grafts fail to restore the activity level to pre-injury levels, resulting in re-tearing in the long run [6]. Current approaches in tissue engineering aim to address these shortcomings. Tissue-engineered grafts eliminate the risks of donor site morbidity and infection associated with autografts, disease transmission risks, and limited graft availability of allografts.

Recently, several tissue-engineered ligament graft substitutes have emerged using natural and synthetic polymers. Replacing tendon or ligament tissue with synthetic grafts with adequate tensile

strength is successful initially. However, they tend to fail over time because of limitations such as mechanical failure, lack of adequate bone-ligament site integration, recurrent instability or device creep [7]. Given the complex structure and peculiar characteristics of ligament tissues like alignment and crimp pattern of collagen fibers, and high tensile strength of ligament tissues, there is a need for a graft that can mimic the native ligament tissue's mechanical and chemical cues of extracellular matrix (ECM) to stimulate cell growth and regenerate native ligament-like tissue biochemically. As a part of this thesis, we investigated the chemical properties of two flexible polyurethane polymers (i.e., LayFOMM60 and Layfelt) to generate 3D printed scaffolds and test their mechanical properties and biocompatibility with human adipose stromal cells (ASCs).

CHAPTER 2

2.1 Tendon and Ligament tissue

Tendons and ligaments are connective tissues made of dense collagenous tissue, connecting muscle to bone and bone to bone, respectively [2, 8]. The primary function of tendons is to transmit forces produced by muscles to bone, to enable movement [2]. Ligaments, on the other hand, act as joint stabilizers. Tendons and ligaments are structurally and physiologically similar, as fibroblasts that produce the ECM develop from common progenitors with similar gene expression profiles [1, 9-15].

2.1.1 Microstructure of Tendons and Ligaments (T/L)

Tendon and ligament tissues are a complex network of cells and the ECM [16]. A significant part of the tendons and ligaments is formed by water, accounting for 50-70% of the tissue weight [2]. The mechanical and biological function of tendons is greatly determined by the composition and organization of the ECM [9, 16, 17].

Extracellular matrix (ECM)

ECM is predominantly composed of collagen fibril arrays [9]. Collagen constitutes approximately 60-85% of the dry mass of the tendon [2, 16, 18-21]. Collagen type I constitutes roughly 95% of the total collagen content of ECM [16]. The remaining 5% are collagen type III, V [17, 19], VI, IX, X and XI [22]. Collagen type I comprises two α1 chains (COL1a1) and one α2 chain (COL1a2), coiled together in a triple helical structure [12]. Its molecules self-assemble into highly organized fibrils to form collagen fibers [19, 23, 24]. These collagen fibrils align at different hierarchical levels, beginning from tropocollagen, fibrils, fibers, fascicles, and finally forming the whole tendon [2, 16]. Collagen in the matrix is cross-linked to form a fiber-like structure that aligns close

to the long axis of the tissue (i.e., the loading direction), conferring high uniaxial tensile strength to the tendon tissue [16, 19, 25]. Collagen type III also forms fibrils but is smaller and less organized, decreasing gradually during development [12, 19]. Compared to collagen type I, collagen type III has lower tensile strength and is predominantly present in scar tissue produced during tendon and ligament repair [26].

Various non-collagenous matrix components like proteoglycans, glycoproteins and glycoconjugates are interspersed between the collagen units throughout the ECM [16]. Although these non-collagenous components form a minor portion of ECM, they play an essential role in ECM function and maintaining its integrity [1]. Proteoglycans enhance the mechanical properties of the tendon tissue, with their concentrations varying within the tissue. They are more abundant in the areas which are subjected to higher compression. Different proteoglycans are present in the tendon; decorin (DCN), aggrecan (ACAN), versican (VCAN), biglycan (BGN), fibromodulin (FMOD), fibronectin (FN), tenascin-C (TN-C) and tenomodulin (TNMD). The most abundant proteoglycan in tendon tissue is decorin, accounting for roughly 80% of the total proteoglycan content. Decorin decorates collagen fibrils and facilitates fibrillar slippage during the tendon mechanical deformation [16, 19, 27]. Aggrecan retains water within the ECM, thereby increasing the resistance of the tissue to the compression [19, 28]. Fibronectin is located on the collagen surface and acts as an adhesive for the cellular population. Thus, it prevents cell slippage during tendon movement and promotes repair and regeneration of tendon tissue. Tenascin-C binds collagen fibers to decorin, thereby ensuring mechanical stability of the ECM [29].

Tendon cells

The tendon cell population is heterogenous, mesenchymal in origin, and poorly defined [16]. At least three distinct tendon cell populations are identified: tenocytes, tenoblasts and tendon

stem/progenitor cells (TSPCs) (Figure 1). These cells reside between long, parallel chains of collagen fibrils and are surrounded by ECM [30]. Tenoblasts are round immature cells which mature to form tenocytes. Tenocytes represent the majority of resident cells in the tendons [26]. They are terminally differentiated, highly elongated, aligned, and specialized fibroblast-like cells that synthesize collagen-rich ECM but have limited proliferative capacity due to lower metabolic activity and lower nucleus-to-cytoplasmic ratio as compared to tenoblasts [19, 31-33]. TSPCs are multipotent stem/progenitor cells that can regenerate into tendon-like tissues [30].

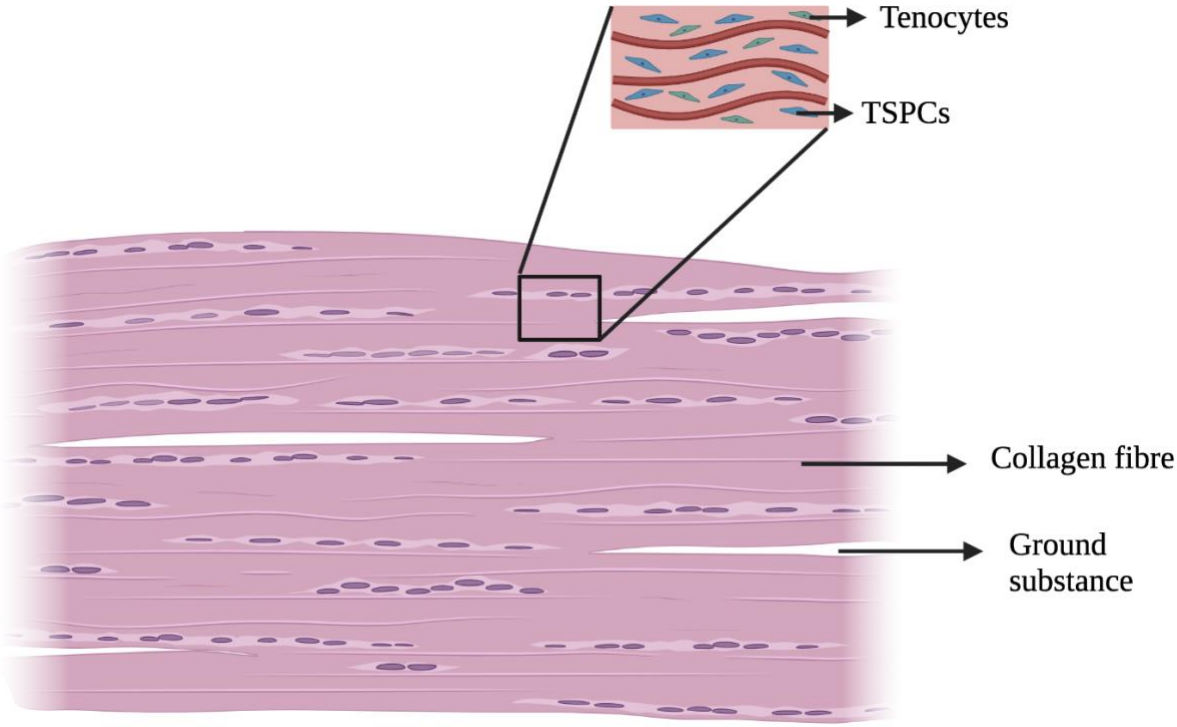

Figure 1- Cellular components and extracellular matrix of tendon

Cell-matrix interaction

The cell-ECM interaction in tendons is complex, dynamic, cyclically linked and influences each other [16]. Tendon cells regulate the formation and organization of the ECM in response to

mechanical and chemical cues [16, 34, 35]. As tensile loading is altered, tenocytes release degenerative enzymes and neo-synthesize ECM components to remodel and adapt the tendon ECM [26]. Collagen fibrils in ECM undergo continuous remodelling in response to mechanical forces. Tenocytes can actively sense mechanical forces, leading to changes in gene expression and ECM organization and secretion [9]. However, ECM controls the cues reaching the cells, creating complex networks and feedback loops linking tendon cells and ECM. The circadian clock greatly influences the cell-ECM complex and mechanical and chemical cues. Specific genes are expressed in anticipation of diurnal mechanical activity [16]. Despite the crucial role of cell-matrix interaction in maintaining matrix homeostasis, it is poorly understood [16].

Collagen fibril arrangement

Microscopically, collagen fibrils in the tendon and ligament are organized in a crimped waveform pattern that differs at different anatomical locations and locations in the same tissue. As the T/L is strained, the crimp pattern of the fibers is straightened [36]. This crimped pattern plays a vital role in determining the mechanical properties of the tendon, as the fibers with a slight crimp angle are mechanically weaker than those with a larger crimp angle [17, 37].

2.1.2 Tenogenic/ligamentogenic genes

Tendon marker genes include scleraxis (SCX), tenomodulin (TNMD), tenascin-C (TNC), and mohawk [35]. Other tenogenic/ligamentogenic lineage indicators are collagen type I and III. Scleraxis (SCX) is an essential helix-loop-helix DNA-binding transcription factor that controls the tendon ECM production [9, 35]. SCX is the earliest known gene marker, is present from the condensation stage of T/L formation, and persists into adulthood [35]. SCX is the key regulator of tenogenic differentiation and is induced by the transforming growth factor β (TGF-β) signalling pathway [35]. *In vitro*, overexpression of SCX has shown to be sufficient to transform

mesenchymal stem cells (MSCs) into tenocytes. SCX directly controls the transcription of COL1a1 and COL1a2.

2.1.3 Tendon and Ligament healing

Like any other tissue in the body, acute injury in ligaments and tendons is followed by rapid initiation of the healing process [2]. This healing process is divided into three overlapping stages with a distinct cytokine profile and cellular processes. These stages are inflammation, proliferation, and remodelling [2, 38, 39].

The inflammatory stage begins immediately after injury and results in clot formation in damaged vessels, activation of inflammatory cells like neutrophils and macrophages, and recruitment of fibroblasts [2, 38]. Platelets and cells release several growth factors at this stage, like TGF-β, insulin-like growth factor-I (IGF-I) and platelet-derived growth factor (PDGF) [2]. TGF-β regulates fibroblasts' migration and proliferation and stimulates the collagen production [2, 40-42]. IGF-I is highly expressed at this stage and functions similarly to TGF-β [42]. PDGF enhances protein and DNA synthesis and stimulates the production of other growth factors, including IGF-I [42]. The proliferative stage is marked by increased cellularity at the site of injury, ECM expansion and deposition of the fibrovascular scar by fibroblasts [13, 38, 42]. High levels of IGF-I and TGF-β attract fibroblasts to the injury site and stimulate ECM production. At this stage, basic fibroblast growth (bFGF) is secreted by tenocytes, ligament fibroblasts and inflammatory cells to promote angiogenesis and cellular proliferation [38, 40, 42]. Vascular endothelial growth factor (VEGF) is also released at this stage to promote the angiogenesis [42].

The remodelling phase starts two weeks after the injury and usually overlaps with the proliferative phase. This phase is marked by a decrease in cellularity, an increase in fibrous content and organization of newly deposited collagen fibrils [42]. Tenocytes/ligament fibroblasts

and collagen fibrils arrange in the direction of mechanical stress. Predominantly, collagen type III is initially secreted in the healing process, which is gradually and slowly replaced by collagen type I over months and years after injury [38, 43]. This newly formed tissue differs from the pre-injury tissue in its mechanical, chemical, biological and ultrastructural properties [39].

2.2 Knee Joint Ligaments

The knee joint is one of the largest, most complex and stressed joints in the human body, along with the hip joint and spine [44]. It is a modified hinge joint which can bear high forces generated during activities like walking, running, sitting, kneeling, etc. [45, 46]. The knee joint comprises bones, tendons, ligaments, menisci, bursae, fat pad, muscles, synovium and articular cartilage [47-49]. It comprises femoro-patellar and tibiofemoral joints, which are joined by a series of ligaments, namely, the medial collateral ligament (MCL), lateral collateral ligament (LCL), anterior cruciate ligament (ACL), and posterior cruciate ligament (PCL) [44, 45]. These ligaments provide passive stability, allowing for complex responses to variable physiological loads subjected to the knee joint. The cruciate ligaments (i.e., ACL and PCL) act as articular stabilizers and prevent anteroposterior translation of the tibia with respect to the femur. These cruciate ligaments are the primary knee joint stabilizers in the sagittal plane and secondary stabilizers in the frontal plane [8, 50]. During knee flexion, primarily, the ACL is responsible for preventing anterior translation of the tibia on the femur. The ACL ligament provides up to 85% of this anterior stability. Due to its crucial role in restraining motion, a complete understanding of the ACL is essential for managing its injuries and improved repair strategies.

The ACL is a crucial knee ligament and is its primary stabilizer. Due to its orientation within the knee resists anterior tibial translations and rotational loads and provides both translational and rotatory constraints [36, 51-53]. It is crucial to understand the ACL anatomy, position, microscopic structure and biomechanical properties if its reconstruction is attempted [54].

2.2.1 Anatomy of the ACL

The ACL is a band-like structure of dense connective tissue connecting the femur and tibia (Figure 2) [52]. It is an intra-articular but extra-synovial structure enveloped by two layers of synovium [53-57]. It receives blood supply from the middle genicular and inferior genicular arteries [54, 58]. The ACL does not have a homogenous blood supply, with the proximal part receiving more blood supply than the distal part and the fibrocartilaginous area being an avascular [8]. It originates from the medial wall of the lateral femoral condyle and runs an oblique course (distal-anterior-medial) through the intercondylar fossa. It then inserts at the medial tibial eminence [53]. The length of the ACL varies from 22-41 mm, with the average being 38 mm [53, 58-60]. Its average thickness ranges from 7-12 mm, with the average being 11 mm [52, 53, 58-61]. A study by Chandrashekhar *et al.* demonstrated differences in length, minimum area and ACL volume between males and females [62], as shown in Table 1.

Sex	Length (mm)	Minimum area (mm^2)	Volume (mm^3)
Male	29.61 ± 2.70	72.91 ± 18.90	2722 ± 706
Female	27.04 ± 2.90	57.32 ± 15.70	1996 ± 530

Table 1- ACL data from a study by Chandrashekhar et al. suggesting ACL anatomical differences between sexes [62].

The ACL has a complex geometry with long fibers at its anterior border and short fibers at its posterior border [36]. It fans out at the insertion site at the tibia with 3.5 times more area than mid

substance [63, 64]. It has its narrowest diameter in the midsubstance with a cross-sectional area of approximately 36 mm^2 in females and 44 mm^2 in males [53, 65]. Fibers at the tibial insertion fan out and form a foot region [53]. The ACL's long axis is 26° ± 6° anterior from the vertical [57], turning the ligament into a lateral spiral. This twist of ACL fibers is because of the orientation of its bony attachments [53]. Its origin on the femur is oriented to the longitudinal axis of the femur. Still, its insertion site is located in the anteroposterior axis of the tibia, giving the ACL an oblique course [53, 56]. The length and orientation of ACL fibers change throughout the motion [53].

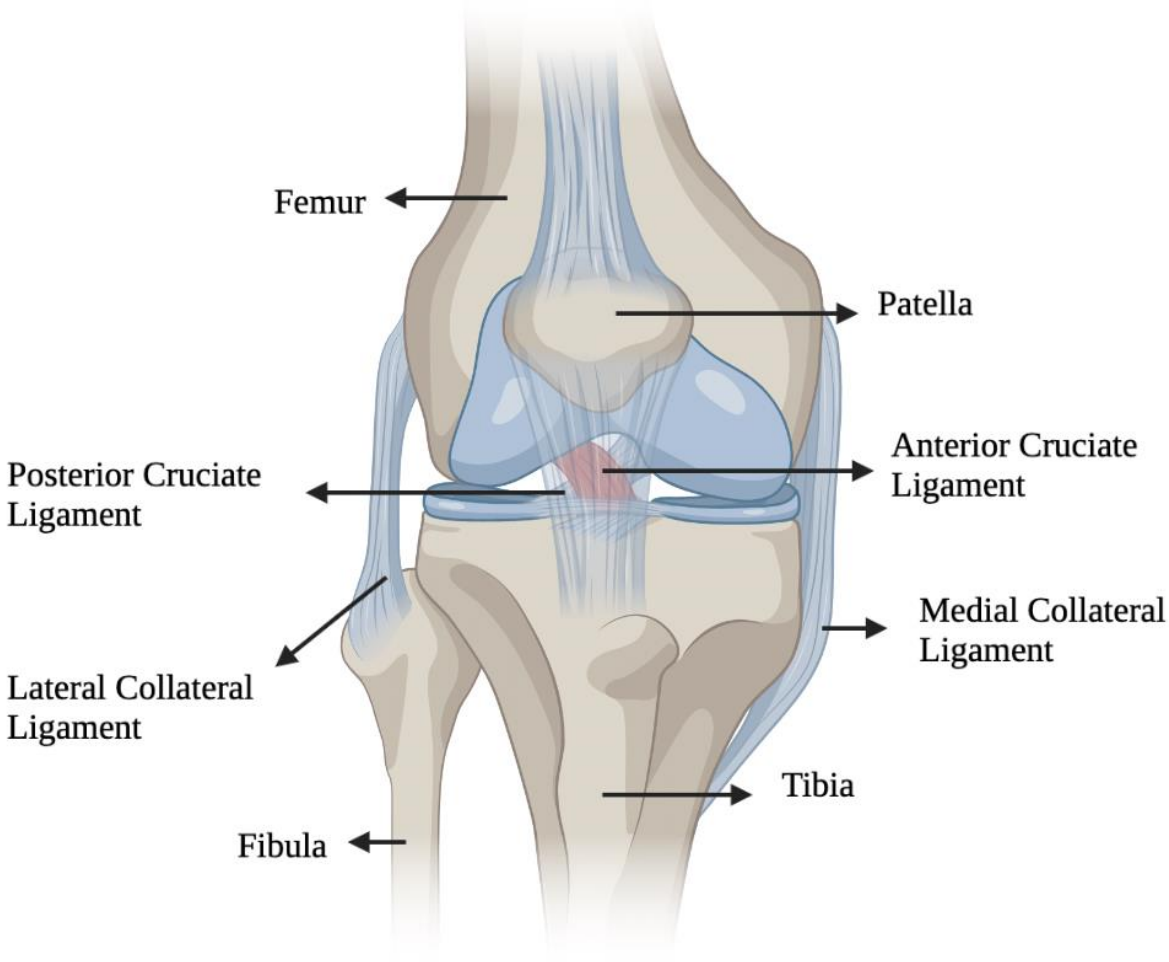

Figure 2- Structure and location of the ligaments of the knee joint.

The fiber bundles of the ACL do not function as a single band of fibers [53] and do not have constant tension throughout its fibers during motion. Instead, it has different tension patterns through different motion ranges [51]. Histologically and anatomically, the ACL ligament does not have distinct bundles, but functionally, it can be divided into two bundles: the anteromedial (AM) and posterolateral (PL) [53, 66]. These bundles were divided based on their tibial insertion [53]. The AM bundle originates from the most proximal part of the femur, inserted at the anteromedial tibial insertion. The PL bundle originates distal to the femoral origin of the AM bundle and inserts on the posterolateral part of the tibial insertion [51, 53, 56, 66, 67]. These two bundles work synergistically to optimize the ACL's restraining function over the range of knee motion [36].

2.2.2 Microscopic structure of the ACL

Microscopically, the ACL is divided into three parts: proximal, middle, and distal [52]. The proximal part is highly cellular, with the majority of cells being round- and ovoid-shaped cells, with some fusiform fibroblasts along with some amount of collagen type II, fibronectin, and laminin glycoprotein [52]. The middle part, also known as the fusiform zone, contains a high density of collagen, elastin and oxytalan fibers and has low cellularity with some fusiform and spindle-shaped fibroblasts with an area of fibrocartilage in the anterior part of ACL [52]. The distal part of the ACL is primarily solid and consists of chondroblasts and ovoid fibroblasts [52]. The fibrocartilaginous zone is found in the anterior portion of the distal third of the ACL [8, 53]. Because of the contact of the ligament with bone in this area, typical ligament fibroblasts are present along with chondrocyte-like cells [53, 56]. Fibrocartilage is a transitional tissue with structural properties of hyaline cartilage and collagenous tissue [8]. The ACL in the tibial and femoral insertion zone has a microstructure typical of a chondral apophyseal enthesis [53]. This

allows the transition of bony tissue to ligamentous tissue and facilitates a gradual change in stiffness to prevent the formation of a zone of stress concentration [53, 56, 57, 67].

Collagen type I fibrils are oriented parallel to the longitudinal axis of the ligament. Typically, collagen type II is not present in ligament and tendon tissues. Still, it is found in the fibrocartilaginous zone of the ACL, indicating the presence of high pressure or sheer stress area [8, 52].

2.2.3 Mechanical properties of the ACL

Ligament and tendon tissues exhibit viscoelastic behaviour, and their load-extension behaviour is dependent on the rate of loading and elongation [68]. Along with the mechanical strength of the collagen fibrils, their mechanical behaviour also depends on the geometrical arrangement of those fibrils and their bundles, the proportion of fibrous constituents, and the surrounding ground substrate [68].

Mechanical properties are defined as the behaviour of the ligament without its insertion site. It can be measured by tensile load testing. To derive a stress-strain curve from the tensile testing, stress is derived by normalizing the applied load by the cross-sectional area of the tissue and strain is derived by normalizing the loaded length to the original unloaded length of the tissue [62]. Young's modulus, ultimate tensile strength and ultimate strain at failure are the essential characteristics to determine the mechanical properties of a ligament. Structural properties, on the other hand, describe the behaviour of the entire bone-ligament-bone complex, that is, the femur-ACL-tibia (FAT) complex in the case of an ACL [68]. Structural properties are measured as a load-displacement response of a tensile loading test, including linear stiffness (the slope of the load-displacement curve), ultimate failure load and energy absorbed at the failure [36]. The mechanical

properties of the ACL vary along its length, so it is usually studied along with structural properties to understand it fully.

In the literature, the mechanical property values for ACLs are inconsistent due to difficulty in assessing the cross-sectional area of an ACL and defining appropriate gauge length. Tensile properties from 3 different studies are listed below in Table 2.

Study	Sex	Elongation at failure (mm)	Strain at failure (mm)	Load at failure (N)	Stress at failure (MPa)	Apparent modulus of elasticity (Mpa)
Woo *et al.*[69]	Male and female combined	9.99	N/A	2160	N/A	N/A
Noyes and Grood [70]	Male and female combined	11.91	0.44	1730	37.8	111
Chandrashekhar *et al.*[62]	Female	7.48±2.56	0.27±0.08	1266±527	22.58±8.92	99±50
	Male	8.95±2.12	0.30±0.06	1818±699	26.35±10.08	128±35
	Male and female combined	8.17±2.41	0.28±0.07	1526±658	24.36±9.38	113±35

Table 2- Mechanical and structural properties of ACL

2.3 TENDON AND LIGAMENT (T/L) INJURIES

Tendon and ligament injuries are among the most common injuries in the body, accounting for more than 50% of musculoskeletal injuries [1, 2]. Each year, around 17 million ligamentous injuries require medical attention in the United States alone, with an associated financial burden of 40 Billion USD [2]. Along with the high economic burden, these injuries significantly compromise a patient's quality of life [2]. T/L injuries are commonly associated with overuse or age-related degeneration [12, 30, 71]. It can range from common sprains and strains to complete tissue tears. The primary function of these tissues is to provide stability and transfer of loads, so their injury results in a loss of function [1]. These connective tissues are bradytrophic, hypovascular and hypocellular, so they have a limited regeneration capacity [26, 72]. Once damaged, they heal very slowly and rarely attain pre-injury mechanical strength and form functionally altered reparative tissue [26, 30]. Currently, no treatment available can restore T/L to its normal condition [12].

2.3.1 ACL Tear

ACL tears account for more than 50% of total knee injuries and affect nearly 200,000 people in the United States each year, posing a financial burden of $7 billion annually [73]. The ACL is a crucial ligament of the knee joint, but it is frequently ruptured during high-impact activities like sports or trauma [52, 74]. With an increase in sports involvement, the incidence of ACL injuries has risen in the last few years [53]. The ACL is the most commonly totally disrupted ligament in the knee [36]. It is associated with several modifiable and non-modifiable risk factors such as female sex, and a younger age group is at higher risk of ACL injury [73]. Female athletes are at increased risk of ACL injury compared to males due to anatomic, neuromuscular, and hormonal

factors [62, 75, 76]. Genetic profile, neuromuscular control, bone morphology, and hormonal profile also play essential roles in [73].

Clinical presentation and diagnosis

ACL tears usually present as acute injuries, associated with a 'pop' and sensation of tearing. An ACL rupture can immediately lead to significant knee instability causing functional instability [36]. If left untreated, it can cause secondary knee damage such as a meniscal tear, intra-articular cartilage injuries [51], and early onset osteoarthritis [36].

Physical examinations are the mainstay of the diagnosis of an ACL injury. The most commonly used diagnostic test during the physical examination for ACL tears are the anterior drawer test, Lachman test, and pivot-shift test [46]. X-ray radiography is done to rule out fracture and dislocation. Magnetic resonance imaging (MRI) is highly recommended due to its high specificity (100%) and sensitivity (97%) for ACL tear diagnosis. It also aids in diagnosing associated damage to menisci, articular cartilage and collateral ligaments. The related injury with an ACL tear influences the treatment approach [77].

Grades of ACL Tears

This grading system guides treatment decisions for surgical reconstruction. Grading of ACL tears is done based on an MRI. ACL tears can be graded as either 1) intact, 2) low-grade partial tear: tear in less than 50% of ligament substance, 3) high-grade partial tear: tear in more than 50% of ligament substance, and 4) complete tear [77]. A partial tear implies that some ligament fibers are disrupted. Its diagnosis is more challenging than a complete tear and usually develops into a complete tear [77]. A low-grade partial tear can be considered for conservative/non-operative treatment. A high-grade partial tear and complete tear present significant joint instability and

should undergo reconstruction. Thus, it is essential to distinguish between low-grade and high-grade partial tears to make a treatment decision [77].

Treatment of ACL Tears

The management of an ACL injury depends on the grade of injury and expected outcomes after the treatment [52]**.** Usually, ACL tear management follows one of two routes: conservative treatment (non-operative therapy) or surgical therapy (operative).

Non-operative/conservative therapy: This involves three months of rest, supervised physiotherapy, anti-inflammatory medications, range of motion training, gradual strengthening of quadriceps, hamstrings, hip abductors and core muscles, and progressive return to activity [73]. However, this treatment might take a long period to heal because of the insufficient self-healing capacity of the ACL. Outcomes of non-operative therapy could result in weakness in the affected area, recurrent injury, and partial loss of function due to scar tissue formation [2].

Operative/surgical intervention: The aim of operative intervention through ACL reconstruction is to restore knee stability, return to normal pre-injury activity and sports, reduce the risk of subsequent arthritis, and restore the native knee anatomy [78]. Surgical reconstruction could be categorized as early or delayed based on the time of surgery after injury. Early reconstruction implies ACL reconstruction within 12 weeks of injury [73]. Per the American Academy of Orthopaedic Surgeons' evidence-based guidelines, an acute ACL tear recommends 12 weeks of non-operative treatment followed by revaluation for the need for surgery. If an ACL reconstruction is indicated, it should be done within five months of the injury to prevent damage to a meniscus, articular cartilage, or both [73]. Studies have shown delayed reconstruction is associated with a higher risk of medial meniscus and medial tibiofemoral cartilage damage [73]. Operative intervention includes surgical reconstruction of the ACL using grafts, either autogenous or

allogenous and is of tendinous origins mainly harvested from the patella, hamstring or quadriceps [79].

2.3.2 ACL Grafts

The surgical reconstruction of ACLs using grafts is a widespread orthopedic procedure. Graft choice depends on several factors like age, donor site morbidity, a baseline level of activity and planned level of future activity. Most commonly, autografts or allografts are being used, patellar and hamstring tendon autografts being the gold standard graft material, have shown a favourable return to play outcomes and preservation of knee functions [73, 79]. Autografts offer several advantages like lower graft failure rate, no risk of disease transmission and immune reaction [79-82]. But these grafts have several limitations like graft site morbidity, insufficient strength and stiffness, limited fixation and compromised host tissue incorporation [83]. There is also a high risk of postoperative morbidities like anterior knee pain, post-operative range of motion restriction, late postoperative graft elongation, patellar tendon shortening or rupture and patellofemoral osteoarthritis, leading to graft failure in 8-10% of ACL reconstruction surgeries [58, 83-89].

Allografts have shown similarities to autografts [78, 79, 90]. There is a rise in the use of allografts from cadavers for ACL reconstruction surgeries as it possesses the advantages of no donor site morbidity, reliable graft size, reduced surgical time, smaller incision, early return to sports and lower postoperative pain [84], and less arthrofibrosis [78, 91]. But allografts have several disadvantages like risks of immunogenic reaction, bacterial infection, disease transmission from graft donor, increased laxity of graft tissue over time resulting in knee laxity, and failure to return to the same level of sports despite an intact graft [84, 92, 93]. Allografts are more successful in older patients with less physical activity and load than in younger patients with more significant physical activity and mechanical load [84].

These inadequacies and significant economic and healthcare burdens associated with currently available graft materials have prompted the development of new tissue engineering approaches to treat these injuries [1].

2.4 TISSUE ENGINEERING

Tendon and ligament healing depends on factors like anatomical location, vascularity, skeletal maturity, and the amount of lost tissue [19, 94]. Ligament injury, like an ACL rupture, results in gap formation in the tissue [1]. Healing is required to bridge this gap, but it does not occur spontaneously as repair processes require infiltration of blood cells to the injury site. Due to poor vascularization of the ACL, ACL injuries cannot heal on their own [19, 95-97]. Although sometimes spontaneous healing occurs at the injury site, it often results in the formation of morphologically, biochemically, and mechanically different from the native ACL. Also, these scar tissues have improper integration with the bone, resulting in fibrous adhesions and inferior functionality of the repaired tissue [19, 98]. Tissue engineering allows treating these injuries by either accelerating the healing process or creating a new construct to act as a ligament graft.

Tissue engineering is a multidisciplinary field which intends to develop biological substitutes to restore, maintain or improve tissue function. The main aim of tissue engineering is to induce regeneration of the tissue. It can be done by two approaches; *in vivo* and *ex vivo*. The *in vivo* approach allows for the self-regeneration of small lesions, and the *ex vivo* approach involves the production of functional tissue that can be implanted in the body. Advancements in tissue engineering approaches have allowed the manufacturing of tissue-engineered substitutes that can modify and maintain living tissue. Tissue engineering techniques now offer potential alternatives

to improve tendon repair and regeneration. Ligaments are highly organized complex 3D structures, and their regeneration usually requires scaffolds, cell seeding, growth factors, or a combination of these techniques. Scaffolds act as templates for cell seeding and provide mechanical stability to the transplant for spatial growth of the regenerative tissue. Commonly used cells for tissue engineering are multipotent cells that are non-immunogenic, easy to isolate and highly responsive to distinct environmental cues. Growth factors usually supplement these scaffolds and cells to drive the differentiation and maturation of cells towards the desired cell type [99, 100].

2.4.1 Scaffolds

Ideal scaffolds should mimic the basic structure of the native tissue and provide short-term mechanical strength to off-load the repair at time zero and some post-operative healing period. Scaffolds used in tissue engineering are categorized into two categories; biological and synthetic [72].

Biological scaffolds

Biological scaffolds are obtained from human, porcine, bovine, or equine tissue. These scaffolds are composed of either collagen or chitosan. These scaffolds are attractive due to their biocompatibility and ECM structure [72]. Collagen scaffolds are increasingly used in tendon tissue engineering as collagen type 1 constitutes more than 60% of the dry weight of tendon. Collagen scaffolds promote cellular proliferation and tissue ingrowth as they are bioactive due to the native structure and surface chemistry [101]. Biological scaffolds are treated before implanting to remove any non-collagenous components to prevent the risk of host rejection, but they still possess chances of eliciting host immune reactions. Also, these scaffolds have poor mechanical properties, low reproducibility, and limited processing ability [72]. Due to these shortcomings, there is increasing interest in using synthetic scaffolds for surgical use.

Synthetic scaffolds

Synthetic scaffolds can act as adequate scaffolds for cellular growth without provoking an inflammatory response in the host [101]. Synthetic biodegradable polymers are often preferentially used due to their reproducible mechanical and physical properties and the control of material impurities. These materials are advantageous because they can be fabricated into various shapes with variable pore frequency and morphology using techniques like additive manufacturing, also known as 3D printing. The most common polymers used in tissue engineering include polylactide (PLA), polyglycolide (PGA), and polylactide-co-glycoside (PLGA) copolymers. One novel class of biomaterial for 3D printing is thermolabile polyurethane and polyvinyl alcohol (PVA) copolymer, which includes LayFOMM60, Layfelt, LayFOMM40, etc. These foamy, highly porous experimental materials do not release any toxic compounds [102]. It is part rubber elastomeric polymer and part soluble PVA [103-105]. They have the potential to be 3D printed as a stiff scaffold and become flexible, as PVA can be washed off with water, leaving behind the more flexible rubber polymer [104, 106, 107]. After rinsing the material with water for 1-4 days, all the soluble PVA is rinsed off, leaving a micro-porous structure with a shore hardness of A60 for LayFOMM60 [108]. These materials are increasingly being used to produce low-cost 3D printed scaffolds using a Fused deposition modelling (FDM) printer [104, 105, 107, 109].

2.4.3 Additive Manufacturing

Fused deposition modelling (FDM), also known as additive manufacturing or 3D printing technique, is an efficient, affordable technology to produce personalized devices and scaffolds with intricate geometries and surface characteristics [109, 110]. In this technique, a thermoplastic material is melted and extruded from the nozzle in a layer-by-layer fashion to build a platform where the temperature is lowered at the end of each layer so that the subsequent layer can fuse to

form a final structure [110]. FDM makes use of computer-aided design (CAD) models in stl. format, which is ‘sliced’ to form a gcode, is a format recognized by the 3D printer. This allows the fabrication of complex 3D structures with controlled external and internal structures like surface geometry, infill density, pore morphology and size [110-113]. A wide variety of polymers and materials can be used in this technique, with the possibility of printing a structure with more than one material using multiple nozzles. One disadvantage of this technique is the use of elevated temperature for printing, thus limiting the scope of biomaterials that can be used.

2.4.4 Cells

Choosing an appropriate cell source is crucial for developing a tissue-engineered graft material, as these cells interact with the native cells and growth factors at the implant site [72]. Most used cells in tissue engineering are patient-derived adult primary cells.

Adult Primary Cells

Adult primary cells represent the tissue's functional unit but have a limited life span, proliferation capability and availability. In the ACL, these cells could be resident tendon or ligament cells. These T/L fibroblasts are difficult to assess along with the challenges mentioned above due to their intrasynovial location [72]. The scope of stem cells is being extensively explored to overcome these challenges. Stem cells are undifferentiated cells with the capacity to self-renew and differentiate into different specialized cells [114].

Embryonic stem cells and pluripotent stem cells

Embryonic stem cells (ESCs) and pluripotent stem cells can differentiate into any somatic tissue. Induced pluripotent stem cells (iPSCs) also have similar potential to differentiate into various cells [115]. Theoretically, the use of ESCs and iPSCs sounds appealing because of their pluripotent nature and auto-reproducibility. However, their practical use is limited due to problems in cell

regulation leading to teratoma formation [116], ethical considerations, immune concerns with ESCs and genetic manipulation difficulties with iPSCs [99, 100, 117]. On the other hand, adult stem cells are immuno-compatible and do not have any significant ethical limitations [99]. For the tissue engineering of mesodermally-derived tissue like tendons and ligaments, the potential of mesenchymal stem cells (MSCs) is increasingly explored.

Mesenchymal stem cells

MSCs are non-hematopoietic stem cells that can differentiate into a spectrum of specialized mesenchymal tissues such as bone, cartilage, tendon, muscle, and adipose tissue [12, 118]. MSCs have the unique ability to secrete growth factors so that they can play an essential role in regenerative medicine. MSCs can be derived from various sources, most commonly from bone marrow. Bone marrow stem cells have been widely used and have shown promising results in the tendon tissue engineering [12]. However, it has several disadvantages like donor site morbidity, painful procurement procedure and low yield (approximately 1 MSC per 10^5 adherent stromal cells) [99]. Due to these significant shortcomings, other MSCs sources like muscle, adipose tissue and bone are being explored by [12]. Another interesting source of MSCs is adipose tissue. Adipose-derived stromal cells (ASCs) are being widely studied due to the abundance and ubiquitous nature of adipose tissue. Adipose tissue can be obtained with minimal patient discomfort and donor site morbidity. Several preliminary studies have shown autologous ASC transplantation to be safe and efficacious in clinal and preclinical studies [99, 100]. Several studies have also shown promising results of ASCs used to heal tendon tissue injuries [118].

Adipose tissue is a highly complex tissue consisting of mature adipocytes (90%) and the vascular, stromal fraction (VSF). The VSF makes up 10% of the total cell population in adipose tissue and

consists of preadipocytes, fibroblasts, vascular smooth muscle cells, endothelial cells, lymphocytes, macrophages [119], monocytes and adipose stem cells [120]. The density and characteristics of ASCs vary with the location of the harvested adipose tissue, type (white vs brown) and species (human vs murine) [121-123]. The isolation and culture of ASCs depend on the isolation technique, culture medium and the mechano-physiological environment like 3D culture, mechanical forces, and degree of oxygenation [99, 124]. Along with its differentiation potential, ASCs also exert their impact by secreting soluble factors Fields[125], such as hepatocyte growth factor (HGF), VEGF, insulin-like growth factor (IGF), and essential fibroblast growth factor (bFGF) [126-128]. These growth factors secreted by ASCs can promote tissue repair and wound healing. So, along with the potential of ASCs in tissue engineering, its use is being widely explored in wound healing, healing of diabetic ulcers, and several dermal lesions [100].

2.4.5 Cross talk between stem cells and biomaterials and the role of scaffold topographic cues on differentiation of stem cells

Applying biomaterials in combination with stem cells is a novel tissue engineering approach to regenerating injured tissue. The main challenge of this strategy is to effectively and accurately promote the differentiation of stem cells into desired cell types. Tenogenic differentiation of stem cells has shown to be dependent on various extracellular matrix (ECM) cues like surface chemistry, elasticity and topography [129]. These ECM cues influence the secretion of paracrine factors from stem cells responsible for the tenogenic differentiation [130]. So, biomimetic biomaterial needs to be designed to mimic physiochemical and biomechanical properties of the tendon to stimulate tenogenic differentiation of stem cells [131].

Cell adhesion is the fundamental step in initiating cell-material interaction to regulate further cell proliferation and differentiation. Biological biomaterials have shown better cell adhesion than synthetic polymers due to their hydrophobic surfaces. The interaction mediates cell adhesion between cell surface receptors and their ligands. One of the crucial adhesion receptors is integrins. Integrins are heterodimeric transmembrane proteins activated by biomaterial surfaces, resulting in a cell adhesion [130].

Role of mechanical properties of scaffold on differentiation of the cell

Cells can sense elasticity and the elastic modulus of the microenvironment and exert contractile forces through integrin-mediated complexes. These interactions between cells and the substrate can direct the tenogenic stem cell differentiation [129]. Research has shown that an elasticity gradient of 40 kPa showed upregulation of proteins that are expressed by tenogenic cells, i.e., scleraxis (SCX), tenomodulin (TNMD), tenascin-C (TNC), and collagen type 3 (COL3), which declined as the elastic gradient of the substrate reached 80kPa. It is unclear how substrates with tensile properties similar to tendons promote differentiation of stem cells towards the tenogenic lineage [132].

Role of fiber alignment of scaffold on differentiation of the cell

Another surface topography that affects the differentiation of stem cells is the fiber alignment of the scaffold. Collagen fibers are aligned along the long axis of the loading in the native tendon tissue [133]. Scaffolds mimicking similarly aligned topographies have been shown to induce tenogenic differentiation *in vitro* [134-143]. Yin *et al.* studied the difference in cell differentiation when human tendon stem cells were seeded on aligned and non-aligned scaffolds [131]. Cells seeded on aligned scaffolds showed higher expression levels of scleraxis, a tendon-specific gene, compared to those on non-aligned scaffolds [140]. These *in vitro* studies suggest that cell

orientation regulated by scaffold fiber alignment impacts cell differentiation. But *in vivo* studies indicate that aligned topography alone might not be enough to drive tenogenic differentiation of the stem cells [132]. Along with the alignment of the collagen fibrils in tendons, another essential feature is the crimp pattern.

Role of crimp pattern of scaffold on differentiation of the cell

Crimp pattern in the tendon collagen fibrils acts as a shock absorber against the mechanical stress tendons are subjected to. *In vitro* studies have been done to mimic this crimp pattern in the scaffold along with the aligned fiber arrangement [144-149]. These studies indicated that cells seeded on such scaffolds exhibited elongated morphology and higher expression of genes of tendon lineage [146-148]. Although this aligned topography with a crimped pattern has shown promising results *in vitro, in vivo* studies still need to be done to confirm these findings.

Indirect effects scaffold topographic cues on differentiation of the cell

Along with these direct impacts of topographic cues on cellular differentiation, they indirectly regulate differentiation by impacting the release of paracrine factors from stem cells. Paracrine factors are the diffusible proteins secreted by the cell to induce changes in the neighbouring [150]. Mesenchymal stem cells release several paracrine factors, such as growth factors like IGF-1, TGF-β, bFGF, VEGF and PDGF, which are responsible for inducing angiogenesis, and fibroblast proliferation and collagen synthesis during tenogenesis. Recent studies have found that the release of these paracrine factors can be modified by modifying the topography of the scaffolds. Differential secretion of paracrine factors has been found with differences in pore size of the scaffold. Macroporous scaffolds (pore size 10-200 μm) and nanoporous scaffolds (5-70 μm) showed differential paracrine effects [151]. Thus, the scaffold should mimic the native tissue in

terms of mechanical strength and recreate the native microenvironment by mimicking proper topography, geometry and porosity.

Thus, in this master's thesis study, we hypothesize that human adipose stromal cells can differentiate into tendon and ligament cells when seeded on LayFOMM60 or Layfelt scaffolds and will drive matrix deposition to act as a ligament tissue substitute. This study aims to determine the mechanical properties of LayFOMM60 and Layfelt scaffolds and assess their compatibility with ASCs to advance the field of tissue engineering application for generating ACL tissue to reduce the economic and healthcare burden.

CHAPTER 3

METHODS

3.1 Scaffold designing and fabrication

This section describes the fabrication of the scaffolds that can act as an ACL graft substitute and a model which can be used in the future to test the effect of uniaxial mechanical forces on the tenogenic differentiation potential of the cell-seeded scaffolds. We 3D printed the scaffolds with LayFOMM60, Layfelt and polylactic Acid (PLA) to seed them with human adipose stromal cells and compare cell adhesion, cell viability, cell metabolic activity, and gene expression of tenogenic gene markers, and protein expression of tenogenic proteins on the cell-seeded scaffolds.

3.1.1 Designing and printing a cylinder-shaped scaffold with windows

LayFOMM60 filament of 1.75mm diameter (MatterHackers, Lake Forest, CA, USA) was purchased to fabricate 3D-printed scaffolds. Before printing, the filaments were heated for 1 hour to remove moisture. A cylindrical scaffold was designed using Autodesk Tinkercad 3D modelling CAD software in stereolithography (.stl) file format and was converted to a RealFlight content format (.g3x) using the Ultimaker Cura 4.3.0 software. The scaffold dimensions were 10 x 2 x 2 mm with a raster angle of 45° and an infill density of 90%. The printing speed was set to 10 mm/s for all the layers, resulting in a total printing time of 20 minutes for each scaffold. The model was 3D printed on a Creator Pro 3D Desktop Printer (Flashforge, Los Angeles, CA, USA). The printer nozzle diameter was 0.3mm. The main printing parameters are found in Table 3. After printing, the scaffolds were washed with double distilled (DI) water for 72 hours to wash off the PVA component. The water was replaced every 24 hours to avoid water saturation with PVA and ensure complete removal of the PVA component from the scaffold.

Print Parameters	LayFOMM60
Print temperature (°C)	215
Bed temperature (°C)	45
Print speed (mm/s)	10

Table 3- Printing parameters for LayFOMM60 scaffold

3.1.2 Redesigning of the scaffold

Due to delamination of the cylindrical scaffold after washing, the scaffold was redesigned into a rectangular-shaped scaffold with gaps between the print. The scaffold was designed with three different fiber alignments, i.e., linear, kinked and S-shaped, to study the effect of different fiber alignments on the differentiation potential of adipose stromal cells.

These scaffolds were printed using white LayFOMM60, Layfelt and polylactic acid (PLA) filaments. LayFOMM60 filament (1.75mm), Layfelt filament (2.85mm) and PLA filament (1.75mm) (MatterHackers, Lake Forest, CA, USA) were purchased for the fabrication of 3D-printed scaffolds. As mentioned above, the same CAD and slicing software was used to design the scaffolds. The dimensions of the scaffolds were 31 x 10 x 0.7 mm with clamps on each side. The measurements for clamps were 6 x 5 x 0.7 mm, and the dimensions for the primary cell seeding area of the scaffolds were 20 x 10 x 0.7 mm, as shown in Figure 3. Gaps were created in the scaffold at an equidistance. The dimensions were similar for all three different fiber alignments and all three scaffold materials.

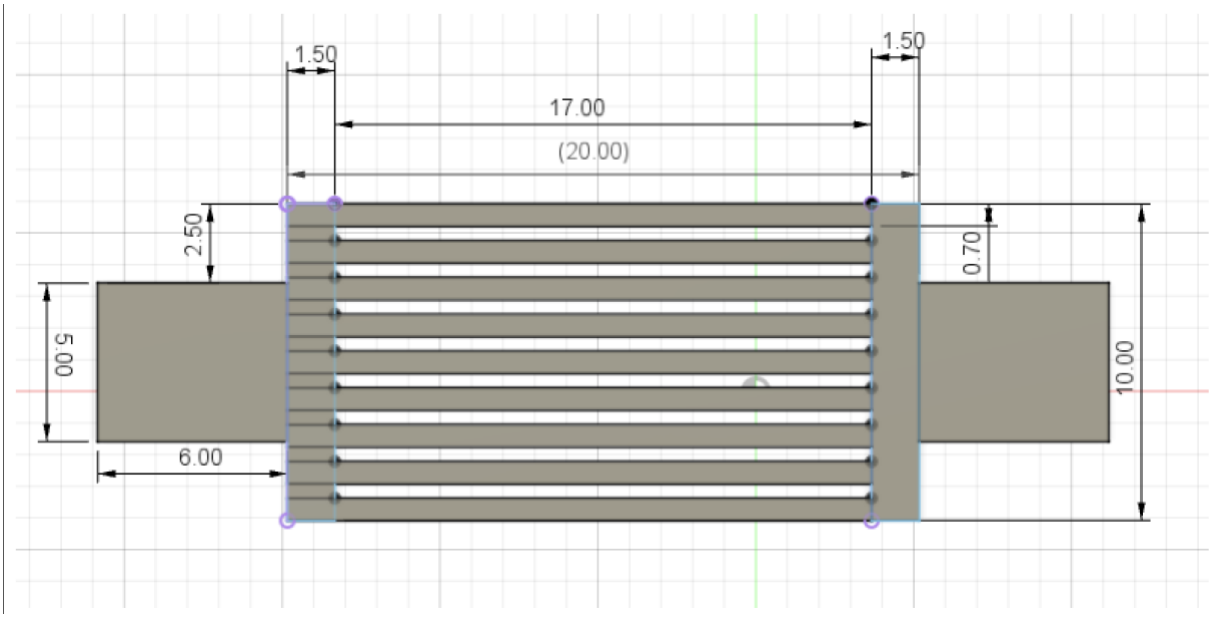

Figure 3- CAD image of the linear designed scaffolds demonstrating all the scaffold dimensions.

The infill density of all the scaffolds was 90%. The printing speed was set to 10 mm/s for all layers, resulting in a total printing time of 25 minutes for each scaffold. The main printing parameters of each material are tabulated in Table 4. Printing parameters were similar for each material's three fiber alignments of the scaffold. LayFOMM60 and Layfelt were heated at 37 °C for 1 hour before printing, and the scaffolds were washed in Double Distilled (DI) water for three days, as mentioned in previous sections. PLA was neither heated before printing nor washed after printing.

The CAD images of all three different fiber alignments are shown in Figure 4.

Print Parameter	LayFOMM60	Layfelt	PLA
Print temperature	210	215	205
Bed Temperature	45	45	70
Print speed (mm/s)	25	25	25

Table 4- Printing parameters of the scaffold used for fabrication of the scaffolds

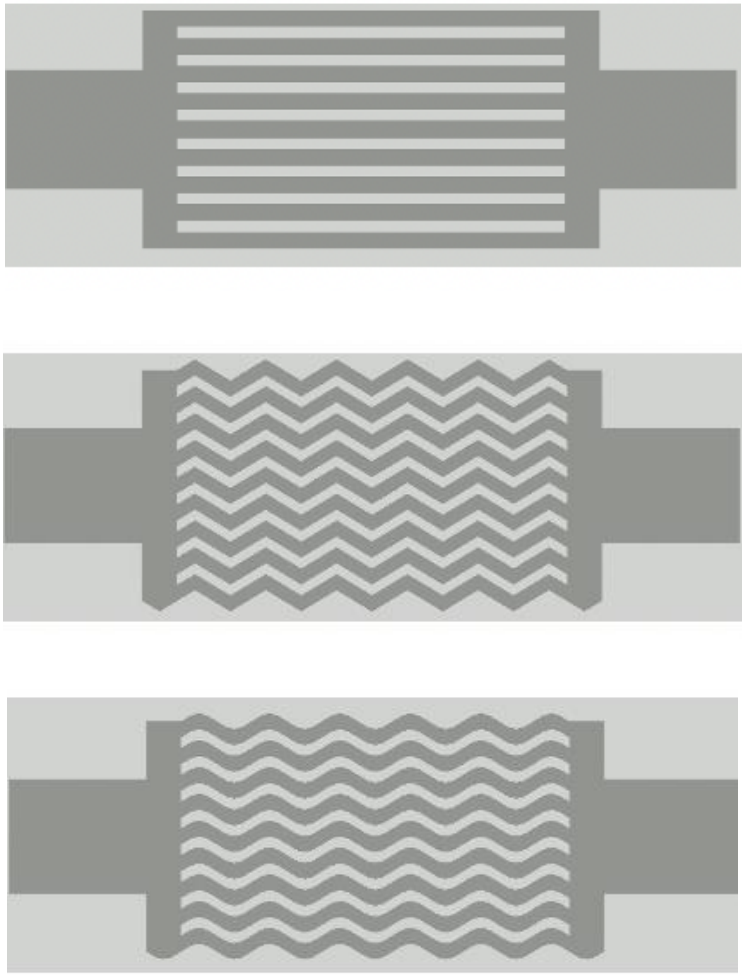

Figure 4- CAD model of scaffolds with three different fiber alignments. a. Linear b. Kinked c. S-shaped

3.2 Material Characterization of LayFOMM60 and Layfelt filament

LayFOMM60 and Layfelt are proprietary materials, so the manufacturer does not disclose the chemical composition and properties. We know that both LayFOMM60 and Layfelt are a combination of polyvinyl alcohol (PVA) and polyurethane in different percentages and that PVA can be washed off from the material. Measuring the difference in weight of the material after all the PVA has been washed off will give an estimate of the percentage of PVA in each material, as shown in Figure 5. Washing off PVA from LayFOMM60 and Layfelt creates micro and nano-

porosities, leading to the material's increased fluid holding capacity. So, measuring the difference in dry weight and wet weight of the material at a particular time point will give an estimate of the fluid holding capacity of the material by comparing these weights for more extended time points. To estimate the degradation of these materials under *in vivo* conditions, we will assess the material's degradation when incubated in distilled water at body temperature.

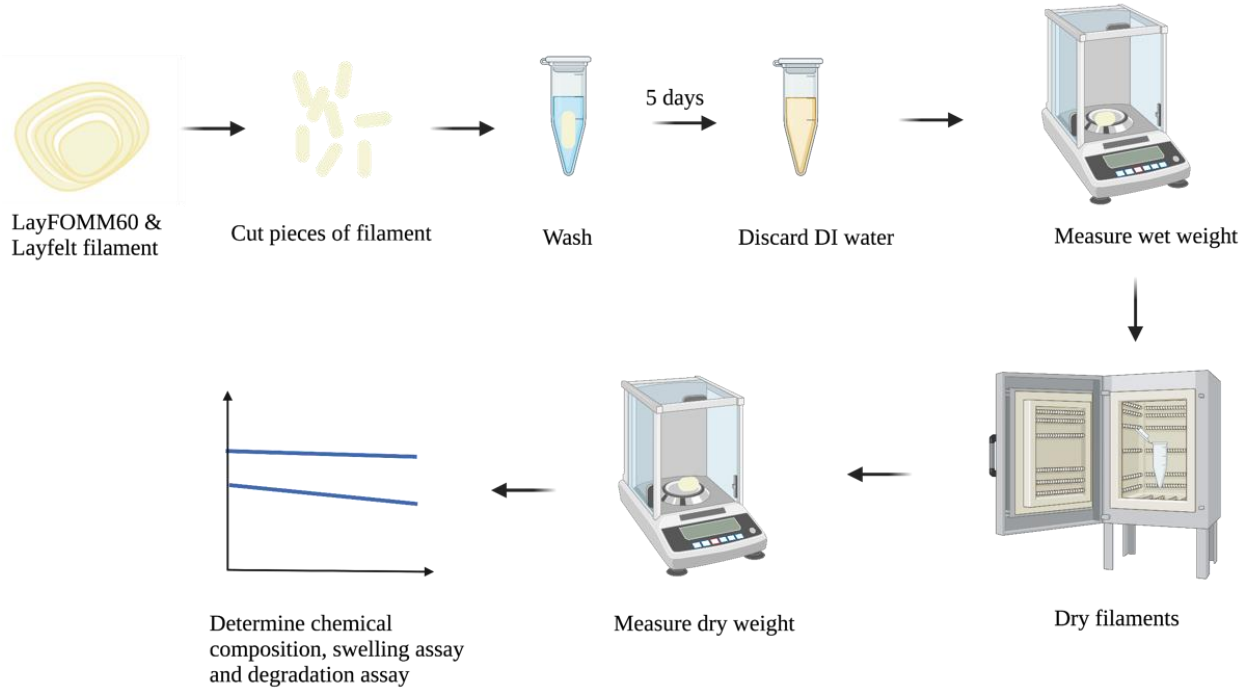

Figure 5- Workflow for the material characterization methodology. The filament was cut into 6 mm pieces and washed for five days to eliminate PVA. After washing wet weight and dry weight of the filament pieces were measured and incubated at 37℃ for the following days. Dry and wet weight were measured at different time points to calculate the filament's fluid holding capacity and degradation profile.

3.2.1 Chemical composition

LayFOMM60 and Layfelt filaments were cut into 6mm pieces and weighed. Each filament was kept in 550 µL of DI water in a 1 mL Eppendorf tube at room temperature. DI water was changed every 24 hours for five days. After five days, filaments were dried overnight at 37°C. After completely drying the filaments, the dry weight of the filaments was measured. The difference in the dry weight after five days of washing and the initial weight of the filament was calculated using the formula below. The difference in weight indicates the amount of PVA lost from the filament.

$$\%\ Difference\ in\ weight = \frac{(Initial\ dry\ weight - Final\ dry\ weight)}{Initial\ dry\ weight} \times 100$$

3.2.2 Swelling assay and degradation assay

After washing the filament for five days to get rid of all the PVA, dry filament pieces were soaked in 500 µL DI water and incubated at body temperature for 90 days. On days 1, 2, 3, 4, 5, 6, 7, and 10, the difference in wet and dry weight of the scaffold was calculated to determine the fluid holding capacity of the filament using the formula below. At the end of 90 days, the dry weight of the scaffold was measured, and the difference in initial dry weight and dry weight after 90 days was calculated to determine the weight loss of the filament using the formulae below, hence degradation of the material.

$$\boldsymbol{Fluid\ holding\ capacity}\ (\%) = \frac{(\boldsymbol{Wet\ weigtht - Dry\ weight})}{\boldsymbol{Dry\ weight}} \times \mathbf{100}$$

$$\boldsymbol{Degradation\ capacity}\ (\%) = \frac{(\boldsymbol{Final\ wet\ weigtht - Initial\ dry\ weight})}{\boldsymbol{Initial\ dry\ weight}} \times \mathbf{100}$$

3.2.3 Tensile testing of the scaffold

The 3D-printed rectangular LayFOMM60 and Layfelt scaffolds printed with three different fiber alignments described above were washed for three days in DI water to eliminate all the PVA before tensile testing. Tensile testing was done on Instron Model 5965 with a 1000 N mechanical load cell. The displacement was set to a maximum of 95 mm, and the test speed was 0.3 mm/s. All the tensile testing was carried out at room temperature. The initial length and width of the scaffold were measured using a calliper.

Stress and strain were calculated from the force and displacement data obtained using the specimen's initial gauge lengths and cross-sectional area. The following equations were used to calculate stress and strain.

$$Stress\ (in\ Pa) = \frac{Force\ (in\ N)}{Area\ (in\ m^2)}$$

$$Strain\ (\%) = \frac{Change\ in\ dimension\ (in\ mm)}{Original\ dimension\ (in\ mm)}$$

Young's modulus is the tangent of the portion of the stress-strain curve under small strain region <10% and was derived as- $Young's\ Modulus = \frac{Stress}{Strain}$

The stress-strain curve directly observed ultimate tensile strength and percent strain at failure.

3.3 Isolation and culture of Adipose stromal cells from human adipose tissue

Human adipose tissues were collected from liposuction and deep inferior epigastric perforator (DIEP) procedures performed at the Royal Victoria Hospital, Montreal, Quebec. Adipose samples were collected with prior patient consent under REB approval number MP-37-2020-5995 (see appendix 1) from the Research Institute of the McGill University Health Center (RI-MUHC). The samples were collected from 10 female donors aged 38-67 years (mean 48 years old). Patient samples were transported to the research laboratory immediately after sample collection. Each piece was weighed and washed vigorously with sterile calcium and magnesium-free phosphate-

buffered saline (PBS; Thermo Fisher, Waltham, MA, USA) supplemented with 2% antibiotic and antimycotic (2% AA is double the recommended strength, Penicillin-Streptomycin and Amphotericin B, Gibco, Burlington, ON, Canada). After washing, the sample was chopped into small pieces and washed vigorously with sterile PBS supplemented with 2% antibiotic and antimycotic (2X AA-PBS) thrice. The chopped tissue was digested for 30 minutes in 0.075% collagenase (by tissue weight) supplemented with 2X AA-PBS. The digest was centrifuged at 1200 x g for 10 minutes. The cell pellet was resuspended in 160 mM NH_4Cl and incubated at room temperature for 10 minutes. This cell suspension was then passed through a 100 μm cell strainer and centrifuged at 300 x g for 5 minutes. The cell pellet was then resuspended in DMEM (Dulbecco's modified Eagle medium standard growth medium: high-glucose) (MilliporeSigma, Burlington, ON, Canada) supplemented with 10% Fetal Bovine Serum (FBS) (MilliporeSigma, Burlington, ON, Canada) and 1% antibiotic-antimycotic (AA), referred to as complete media. The cell suspension was seeded in 10 mL complete media in a T-75 flask and cultured at 37°C in a humidified cell culture incubator with 5% CO_2. After 24 hours, adhered cells in T-75 cell culture flasks were washed twice with sterile PBS, and 10 mL of complete media was added to the flask. The culture was maintained at 37°C, and 10 mL of fresh media was added every three days. The cells were passaged until passage 4.

3.4 Cell seeding on the scaffold

Adipose stromal cells at passage four were washed using sterile PBS and detached using 0.05% Trypsin-EDTA (Gibco, Burlington, ON, Canada). Detached cells were collected and centrifuged at 500 x g for 5 minutes. The cell pellet was resuspended in complete media. LayFOMM60, Layfelt and PLA scaffolds were prepared for cell seeding. The scaffolds were washed with 70% ethanol for 15 minutes and were put under UV light for 30 minutes. Before cell seeding, the

scaffolds were stored in sterile PBS. The cells were seeded onto the scaffolds at a density of 500,000 cells per scaffold in a 5 mL syringe. Cells (5×10^5) were present in 3 mL media in a 5 mL syringe fitted with a sterile stopcock. One scaffold was inserted in each syringe and kept perpendicularly inside the culture incubator. All the syringes were rotated 90° every 45 minutes to ensure uniform cell distribution and adhesion. The total time for cell adhesion inside the culture incubator was 3 hours. At the end of 3 hours, all the contents from the syringe, including leftover culture media and the scaffold, were transferred to the corresponding wells in a 12-well suspension plate, as shown in Figure 6.

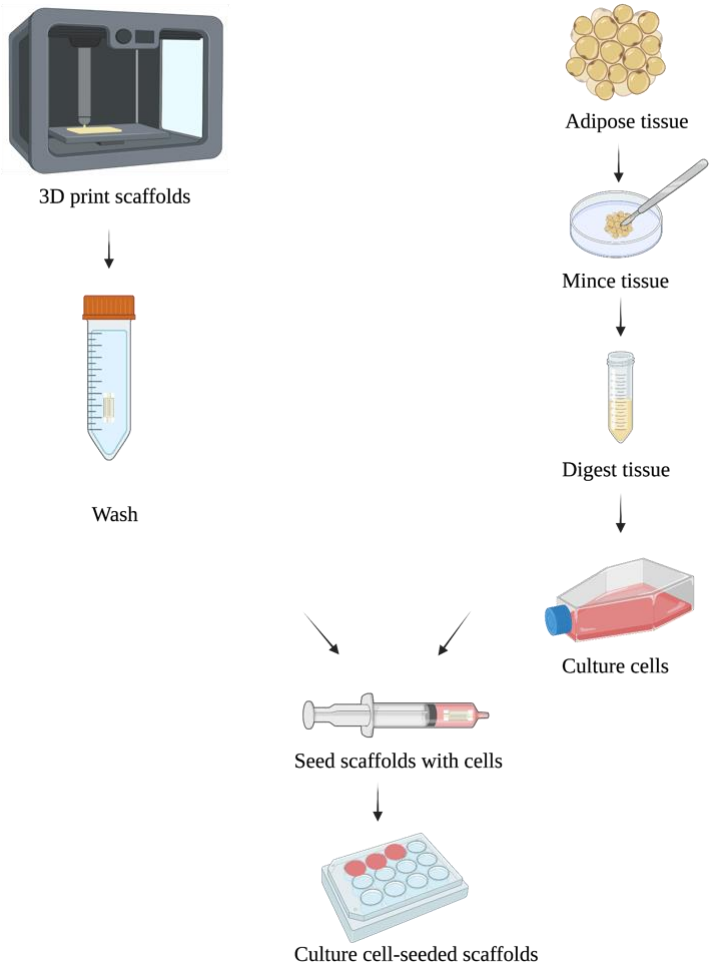

Figure 6- Schematic showing preparation of 3D printed scaffolds and subsequent adipose cell seeding of the scaffolds in a 12-well suspension plate.

3.4.1 Cell adhesion

After transferring all the contents of the syringe into the suspension wells after 3 hours, the number of remaining cells was counted in the left-over media. The cells in the left-over media were the number of cells that did not attach to the scaffold during the 3-hour incubation time. % Cell adhesion was calculated using the following equation-

$$Cell\ adhesion\ (\%) = \frac{Number\ of\ initial\ cells\ seeded - Number\ of\ cells\ in\ left\ over\ media}{Number\ of\ initial\ cells\ seeded} \times 100$$

3.4.2 Cell viability and metabolic assay

After seven days in culture, cell viability of adipose stromal cells on the scaffolds was assessed using a LIVE/DEAD™ assay (Invitrogen, Carlsbad, CA, USA) prepared in sterile PBS as per the manufacturer's instructions. 500 μL of the prepared LIVE/DEAD solution was added to the cell-seeded scaffolds and incubated for 15 minutes at 37°C. After 15 minutes, the LIVE/DEAD solution was discarded, and sterile PBS was added. An Olympus IX81 inverted fluorescence microscope using a 10x objective with MAG Biosystems Software 7.5 (Photometrics, Tucson, AZ, USA) was used to capture images at 10X magnification.

Cell metabolic activity was also determined on day seven by an AlamarBlue™ assay (ThermoFisher, ON, Canada) prepared in Dulbecco's Modified Eagle Medium (DMEM) as per the manufacturer's instructions. AlamarBlue™ reagent was added to the complete media at a 1:9 ratio to get a 10% Alamar blue solution. 500 μL of the prepared solution was added to the cell-seeded scaffolds and incubated at 37°C for 2 hours. 150 μL of the solution was transferred to a 96-well plate. The sample's fluorescence was measured using a Tecan M200 Pro microplate reader (Tecan, Mannedorf, Switzerland) at an excitation of 570 nm and emission of 600 nm.

3.4.3 Gene expression

Quantitative reverse transcriptase mediated polymerase chain reaction (RT-qPCR) was performed on the cell-seeded scaffolds on day 7 to assess the tenogenic gene expression. TRIzol™ (Invitrogen, Carlsbad, CA, USA) was used to extract RNA per the manufacturer's instructions. Jscript reagent (Quantabio, Beverly, MA, USA) was used for the reverse transcription of 500 ng of RNA into cDNA. Quantitative RT-PCR was performed on the StepOne Plus Real-Time PCR System (Applied Biosystems, Foster City, CA, USA) using PerfeCTa SYBR Green Reagent (Quantabio, Beverly, MA, USA). Amplification of collagen type I (*COLIA1*), collagen type III (*COL3A1*), and scleraxis (*SCX)* was quantified (Life Technologies Inc., Carlsbad, CA, USA). The sequences of the forward and reverse primers used for the gene expression are mentioned in Table 5. Gene expression was normalized to the house-keeping gene β-actin, and relative fold-expression for each target gene was evaluated using the ΔΔCT method. Undifferentiated adipose stromal cells before cell seeding at passages four were used as the control.

Target gene	Forward primer (5'—3')	Reverse primer (3'—5')
COL1A1	GGTGATGCTGGTCCTGTTG	ATCGTGAGCCTTCTCTTGAG
COL3A1	CCCAGAACATCACATATCAC	CAAGAGGAACACATATGGAG
SCX	AGAACACCCAGCCCAAAC	TCCTTGCTCAACTTTCTCTGGT

Table 5- Sequence of the Forward and Reverse Primers used for qPCR

3.4.4 Immunofluorescence and protein analyses

After 21 days in culture, the cell-seeded scaffolds were treated with permeabilization buffer (PBS, 1% Bovine Serum Albumin, 0.1% Triton-X100) for 45 minutes. Permeabilized samples were then incubated overnight with primary antibodies against tenomodulin (1:200, Abcam, Cat no.- ab203676, Cambridge, MA, USA), Scleraxis (1:200, Abcam, Cat no.- ab58655), Collagen type 1

(1:200, Abcam, Cat no.- ab6308) and Collagen type 3 (1:200, Abcam, Cat no.- ab7778) at room temperature. Samples were washed three times in PBS and then incubated with Alexa Fluor 488 donkey anti-rabbit IgG (1:1000, Invitrogen, Cat no.- A21306) for samples incubated with Tenomodulin and Collagen type 3 and with anti-mouse IgG (1:1000, Invitrogen, Cat no- A21422) for samples incubated with Collagen type 1 and Scleraxis, at room temperature for 1 hour. Samples were washed with PBS and mounted using Fluoroshield with DAPI (SigmaAldrich, Oakville, ON, CA) and visualized on an EVOS M5000 Microscope (ThermoFisher, ON, Canada).

CHAPTER 4

RESULTS

4.1.1 Material characterization of the LayFOMM60 and Layfelt filament

The initial average dry weight for LayFOMM60 was 16 ± 0.75 mg (Mean ± SD), and that for Layfelt was 16 ± 0.71 mg. After five days of washing with DI water, the average wet weight for LayFOMM60 was 18.5 ± 0.84 mg and that for Layfelt was 15.95 ± 0.49 mg. The average dry weight after five days of washing for LayFOMM60 was 11.83 ± 0.48 mg and that for Layfelt 8.48 ± 0.15 mg, indicating 27% weight loss in LayfOMM60 filament and 47% weight loss in Layfelt filament (Figure 7).

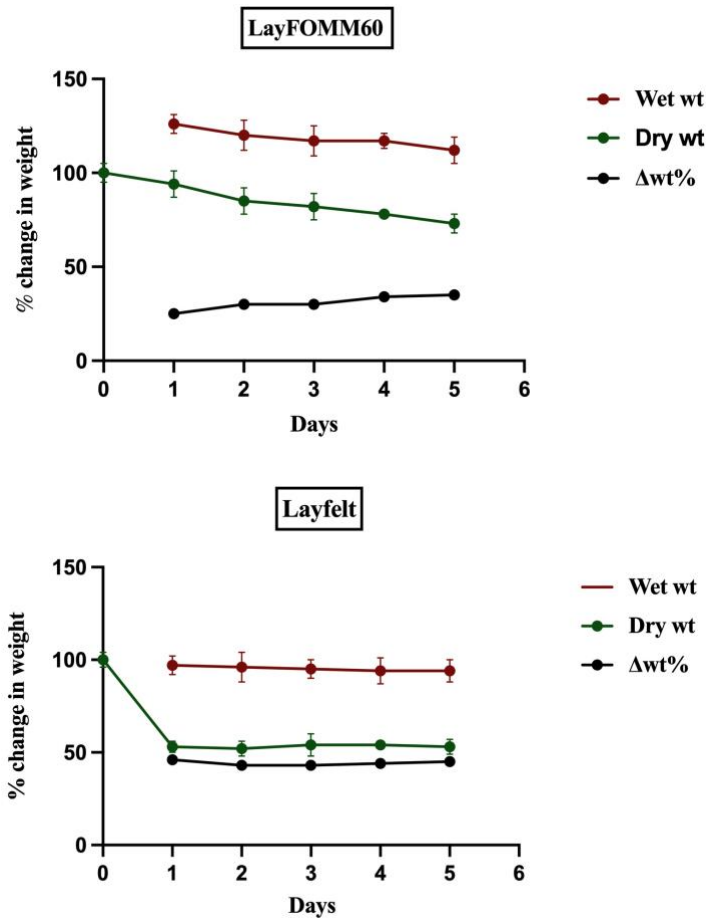

Figure 7- Chemical composition of LayFOMM60 and Layfelt filament. Wet weight represents the weight of the filament after being soaked in DI water. Dry weight means the weight of filament after drying the wet filament overnight. ∆wt% is the percentage difference in the filament's dry and wet weight compared to its dry weight. Both dry and wet weight show low standard deviations, indicating high repeatability. Error bars represent ± SD.

After washing LayFOMM60 and Layfelt filaments, these filaments were kept at room temperature, and the difference in dry weight and wet weight on 1,3,4,5,6,7,10 and 90 days are mentioned in Table 6.

Days	LayFOMM60		Layfelt	
	Dry weight (mg)	***Wet weight (mg)***	***Dry weight (mg)***	***Wet weight (mg)***
1	11.83 ± 0.48	17.22 ± 0.42	8.48 ± 0.15	15.23 ± 0.22
3	11.98 ± 0.05	17.08 ± 0.92	8.53 ± 0.54	15.20 ± 0.54
4	11.98 ± 0.05	16.53 ± 0.36	8.95 ± 0.21	14.88 ± 0.21
5	11.80 ± 0.34	16.95 ± 0.62	8.58 ± 0.15	15.78 ± 0.29
6	11.33 ± 0.63	16.50 ± 0.91	8.55 ± 0.31	15.33 ± 0.29
7	11.40 ± 0.42	16.08 ± 0.57	9.15 ± 0.13	16.10 ± 0.34
10	11.03 ± 1.02	16.28 ± 1.29	8.43 ± 0.15	15.60 ± 0.53
90	10.68 ± 0.19	16.23 ± 0.19	8.84 ± 0.30	15.36 ± 0.69

Table 6- Dry weight and wet weight of the filaments at 1,3,4,5,6,7,10, and 90 days

The initial average dry weight for LayFOMM60 was 11.83 ± 0.48 mg and for Layfelt was 8.48 ± 0.15 mg. After ten days of incubation, the average wet weight of LayFOMM60 was 16.28 ± 1.29 mg and that for Layfelt was 15.60 ± 0.53 mg. The average dry weight after ten days for LayFOMM60 was 11.03 ± 1.02 mg and for Layfelt was 8.43 ± 0.15 mg indicating a 35% average swelling ratio in LayFOMM60 and 45% in Layfelt. After 90 days of incubation, the average dry weight was 10.68 ± 0.19 mg for LayFOMM60 and 8.84 ± 0.30 mg for Layfelt scaffold, indicating an insignificant weight loss over the 90 days (Figure 8).

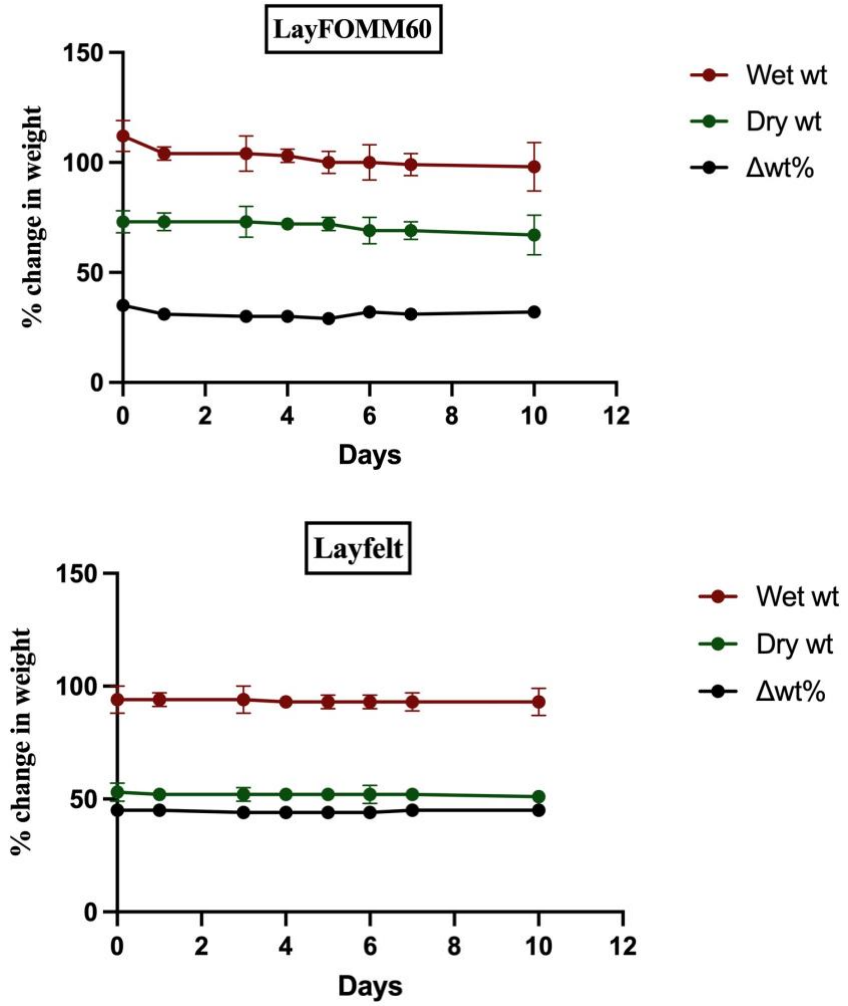

Figure 8- Swelling assay and degradation profile of LayFOMM60 and Layfelt filament. Wet weight represents the weight of the filament after being soaked in DI water. Dry weight means the weight of filament after drying the wet filament overnight. Δwt% is the percentage difference in the filament's dry and wet weight compared to its dry weight. Both dry and wet weight show low standard deviations, indicating high repeatability. Error bars represent ± SD.

4.1.2 3D printing of LayFOMM60 and Layfelt scaffolds with different fiber alignments

Scaffolds were 3D printed in 3 different fiber alignments. There was a clear-cut differentiation in CAD designs of kinked and s-shaped, which is not very evident in the 3D printed scaffolds, shown in Figure 9.

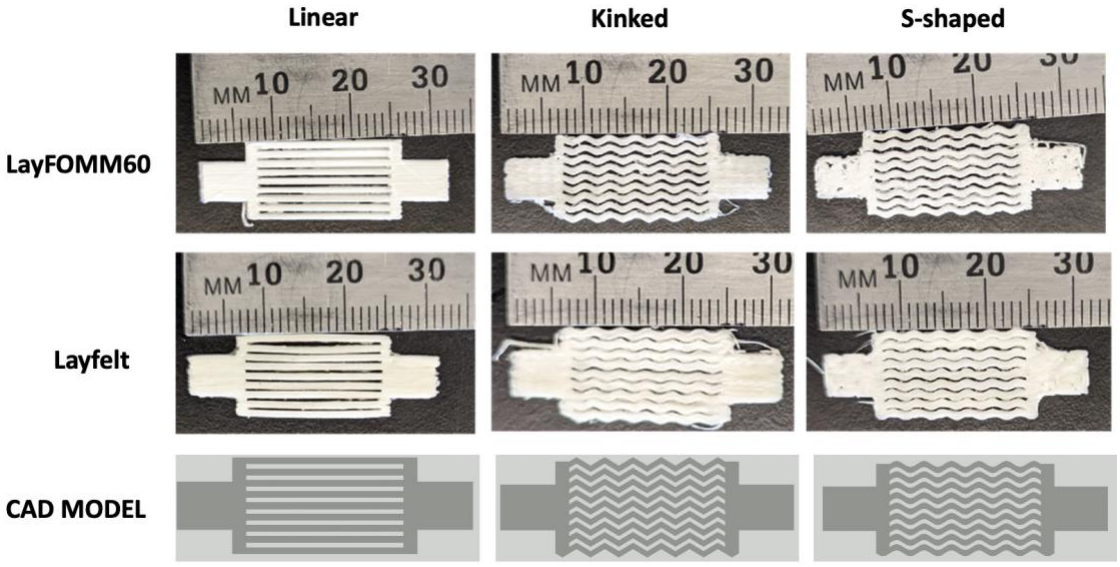

Figure 9- Representative images of 3D printed scaffolds using LayFOMM60 and Layfelt filament. CAD models are included to highlight the difference in fiber alignment in different pattern designs.

4.1.3 Tensile properties of rectangular 3D printed scaffolds

Several LayFOMM60 and Layfelt scaffolds did not reach failure. Stress-strain curves for all materials are shown in Figure 10. Individual curves were used to determine the Apparent Modulus, Ultimate Tensile Strength (UTS) and the % strain at failure. The stress-strain behaviour of the polymers did not follow the typical tensile curve with an elastic region followed by a plastic region. The linear portion commonly seen in low strain regions was not distinct for LayFOMM 60 and Layfelt.

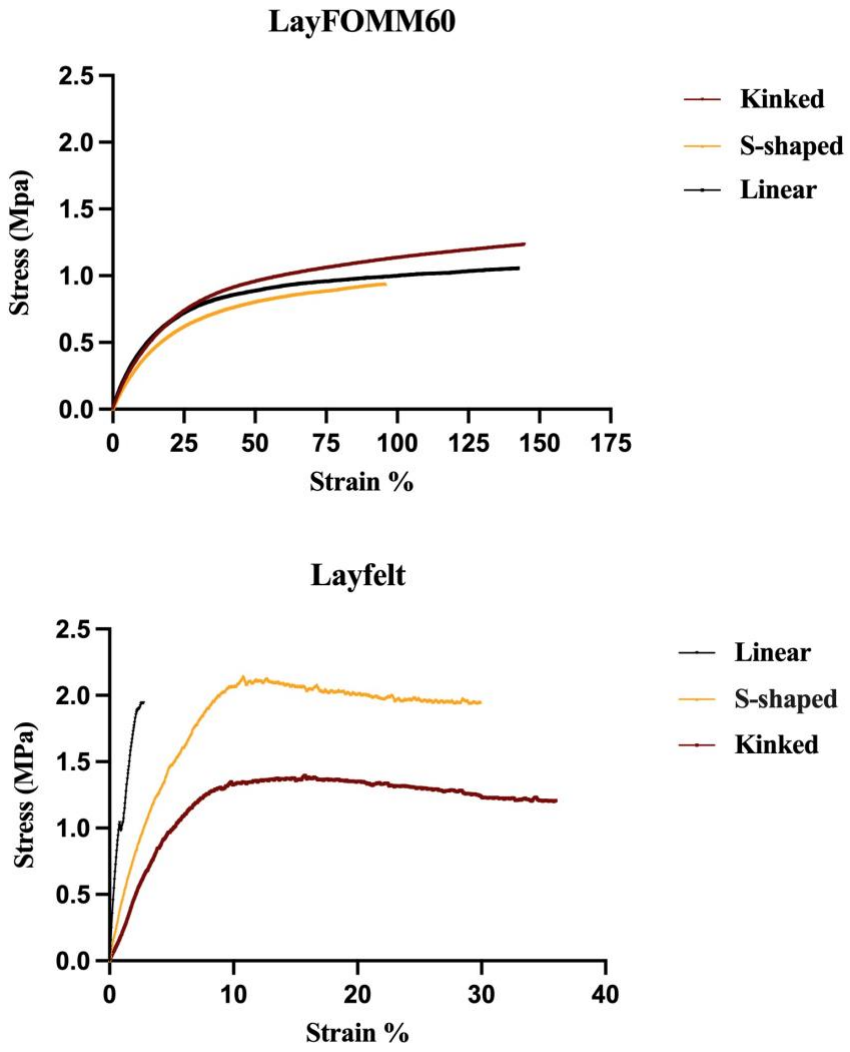

Figure 10- The stress-strain curves for LayFOMM60 and Layfelt scaffolds with different fiber alignments (n=3).

The calculated UTS, Apparent Modulus and percentage strain at failure are shown in Figures 11 and 12, with corresponding results in Table 7. In the case of Layfelt, fiber alignment had a significant effect on Apparent modulus. Apparent modulus was also significantly different between LayFOMM60 and Layfelt, but fiber alignment did not significantly differ within LayFOMM60. Ultimate tensile strength was significantly different between LayFOMM60 and

Layfelt but not between different fiber alignments in LayFOMM60 and Layfelt. % Strain of failure was significantly higher for LayFOMM60 for all fiber alignment than Layfelt.

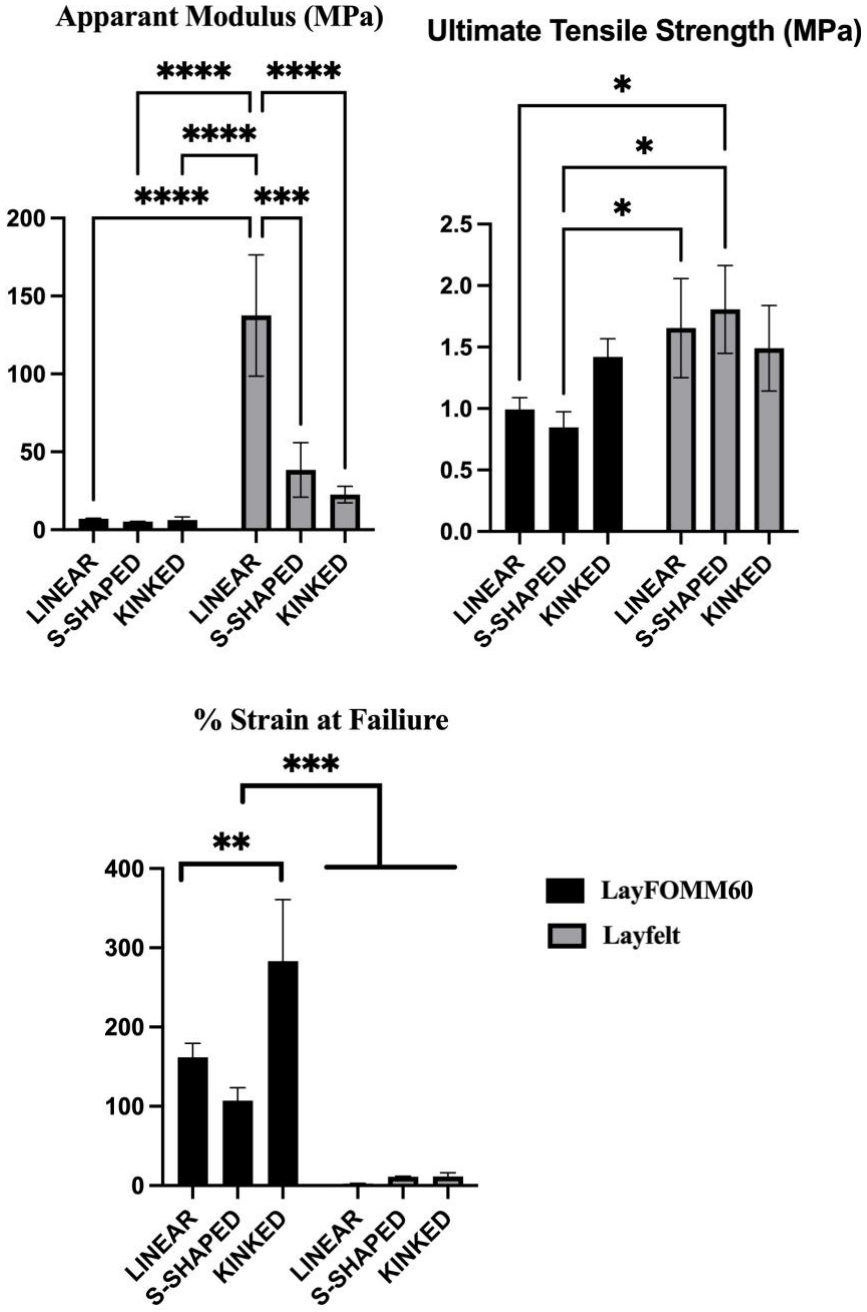

Figure 11- Mechanical properties of LayFOMM60 and Layfelt at three differing fiber alignments: linear, s-shaped, and kinked. (A) Apparent Modulus; (B) Ultimate Tensile Strength; (C) % strain at failure. The data shown represent the Mean ± SD.

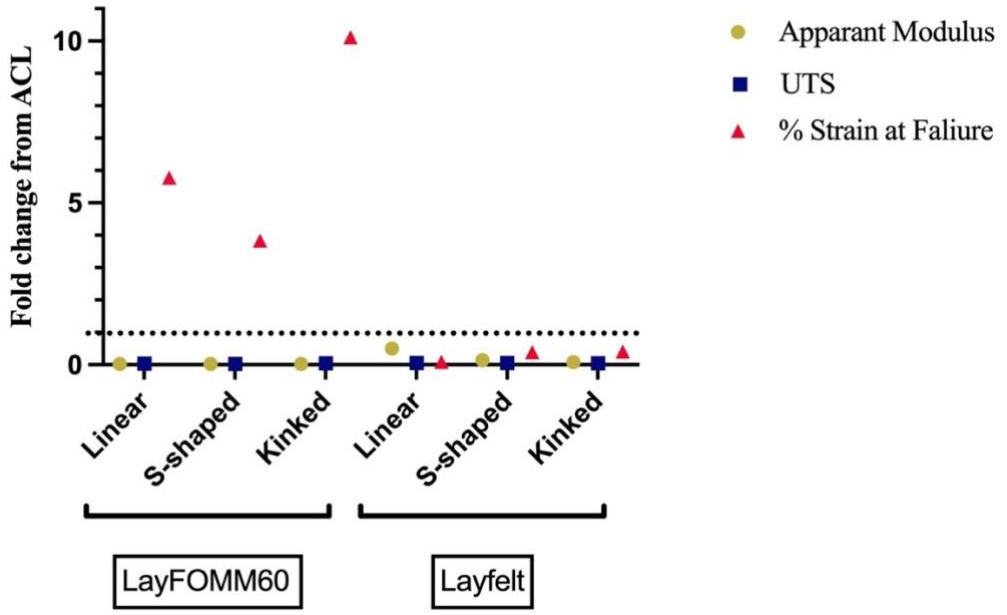

Figure 12- Percentage change of values compared to published native ACL mechanical properties. Linear, S-shaped and Kinked are three different fiber alignments. Apparent Modulus values are shown in the yellow circle, UTS is a blue square and strain at either fail

Material	Fiber alignment	Ultimate tensile strength (Mpa)	Apparent Modulus (Mpa)	% Strain at failure
LayFOMM60	***Linear***	0.9925 ± 0.095	7 ± 0.438	161.74 ± 17.74
	S-shaped	0.846 ± 0.128	5.20 ± 0.289	107.28 ± 16.18
	Kinked	1.42 ± 0.147	6.23 ± 2.03	283.191 ± 77.59
Layfelt	***Linear***	1.655 ± 0.403	137.50 ± 38.89	2.52 ± 0.29
	S-shaped	1.80 ± 0.356	38.36 ± 17.52	11.05 ± 0.75
	Kinked	1.49 ± 0.348	22.55 ± 5.30	11.48 ± 4.84

Table 7- Calculated values of UTS, Apparent Modulus and percentage strain at failure for LayFOMM60 and Layfelt scaffolds

4.2 ASCs seeding on LayFOMM60 and Layfelt scaffolds

4.2.1 Cell adhesion

Significant differences in cell adhesion were observed after seeding onto linear LayFOMM60, Layfelt and PLA scaffolds (Figure 13, $p < 0.05$). PLA scaffolds had the highest adhesion at 65 ± 15.4%, while Layfelt scaffolds had the lowest at 55 ± 12.2%. Layfelt had the cell adhesion of 58 ± 10.8%.

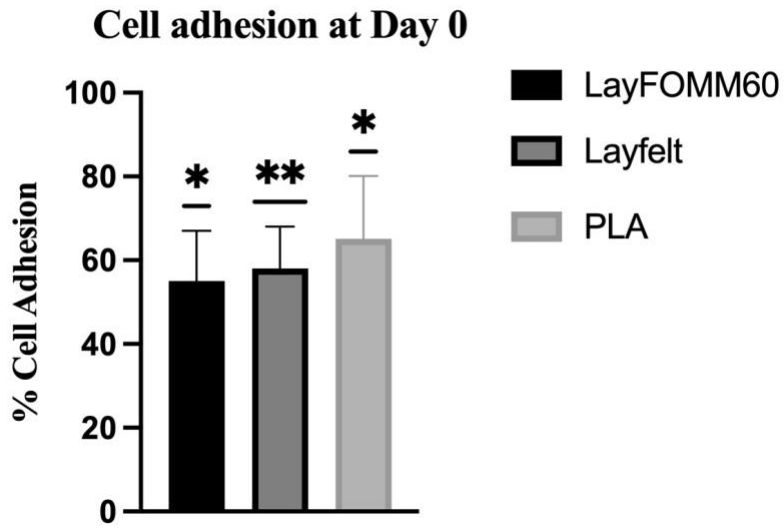

Figure 13- Adipose stromal cells (ASCs) cell attachment at day 0 for linear LayFOMM60, Layfelt and PLA scaffolds.

4.2.2 Cell viability

Cell viability was assessed via LIVE/DEAD^{TM} assay on day 7 of cell seeding (N=3). Representative images of scaffolds cultured with ASCs indicate similar viability among all

conditions. All the scaffolds show a good number of green stained cells indicating live cells. Dead cells are not present in any scaffolds (Figure 14).

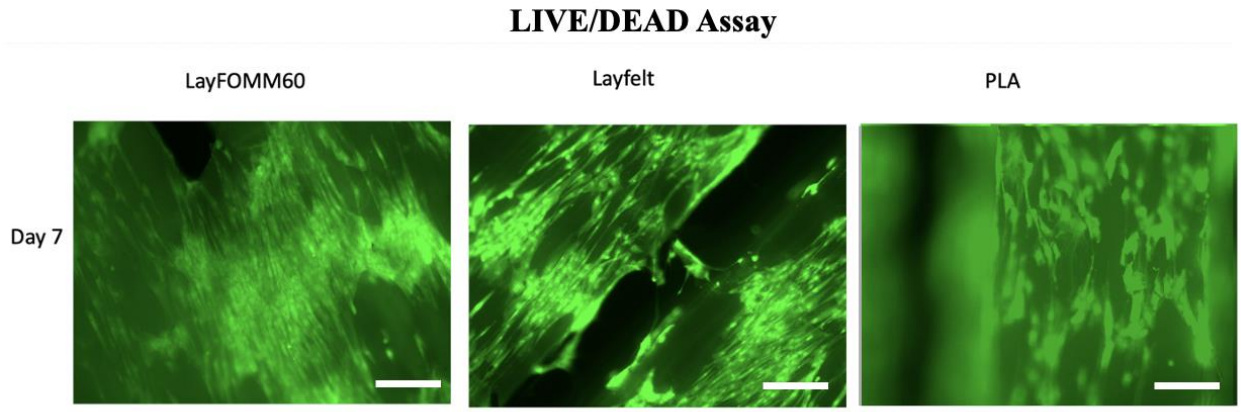

Figure 14- Cell viability on linear LayFOMM60, Layfelt and PLA scaffolds cultured with adipose stromal cells (ASCs). LIVE/DEADTM Assay was performed after seven days of culture. Live cells are shown in green (Calcein AM) dead cells are shown in red (ethidium homodimer). Representative images (N=3) show that the number of dead cells in all conditions in the cultured membrane is negligible. Scalebar = 250µm, magnification 10X.

4.2.3 Cell metabolic activity

To assess whether the viable cells on the scaffolds were metabolically active, cell metabolic activity for all cell-seeded scaffolds was measured with an AlamarBlue™ assay on day 7 of culture. Figure 15 demonstrates that ASCs seeded on PLA scaffolds are significantly more metabolically active than that on LayFOMM60 and Layfelt scaffolds, culminating in the percent AlamarBlue™ reduction of 162.2 ± 40%, 100.0 ± 1.1%, and 69.5 ± 3.5%respectively.

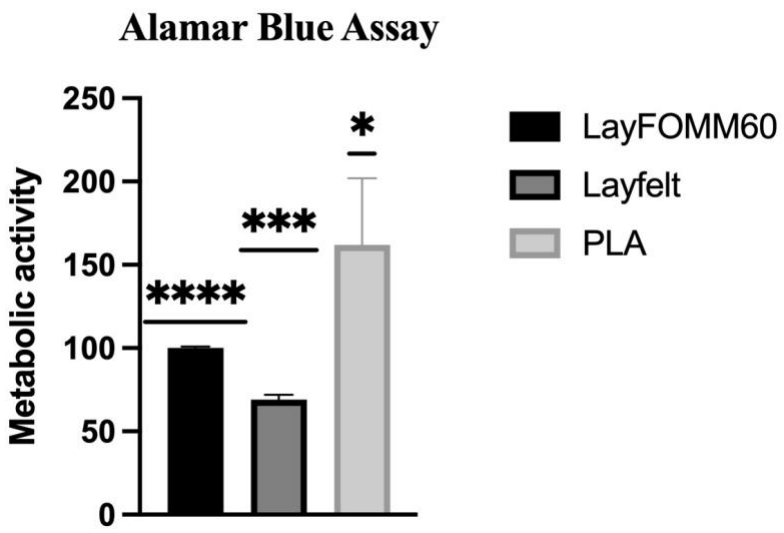

Figure 15- Metabolic activity quantified via AlamarBlue™ assay at seven days of culture. Error bars represent mean ± SD.

4.2.4 Gene expression

Gene profile of ASCs and differentiation of ASCs on different scaffold material toward the tenogenic phenotype were assessed via expression of tenogenic gene markers collagen type I, collagen type 3, and Scleraxis at seven days of culture. Figure 16 shows that ASCs cultured on all three scaffolds for seven days showed significantly lower expression of collagen type 1 and collagen type 3 compared to undifferentiated ASCs at P4. But there were marked increases in expression of Scleraxis.

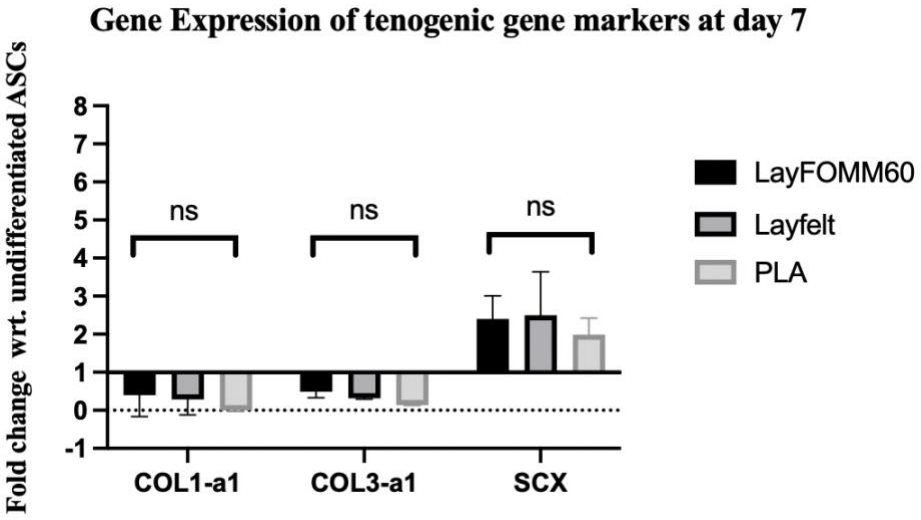

Figure 16- Fold change of tenogenic gene markers in ASCs when seeded on LayFOMM60, Layfelt and PLA compared to undifferentiated ASC at P4. Error bars represent average ± SD.

The fold change of all the gene markers on each scaffold is listed in Table 8.

Scaffold material	Collagen type 1	Collagen type 3	Scleraxis
LayFOMM60	0.395 ± 0.556	0.486 ± 0.157	2.4 ± 0.608
Layfelt	0.286 ± 0.403	0.316 ± 0.021	2.49 ± 1.142
PLA	0.003 ± 0.03	0.138 ± 0.011	1.99 ± 0.429

Table 8- Fold change of tenogenic gene markers in ASCs when seeded on LayFOMM60, Layfelt and PLA as compared to undifferentiated ASC at P4.

4.2.5 Tenogenic matrix formation

The distribution of tenogenic proteins like collagen 1a1, collagen 3a1, tenascin-c and tenomodulin was assessed on cell-seeded LayFOMM60 and Layfelt scaffolds using immune fluorescence after

21 days of culture (Figure 17). All scaffolds displayed some autofluorescence, but cells showed specific staining above acellular background levels on all coating types. There was an even distribution of tendon-like matrix deposition on both the scaffolds; Phalloidin staining (red-orange) was used to demonstrate cell morphology.

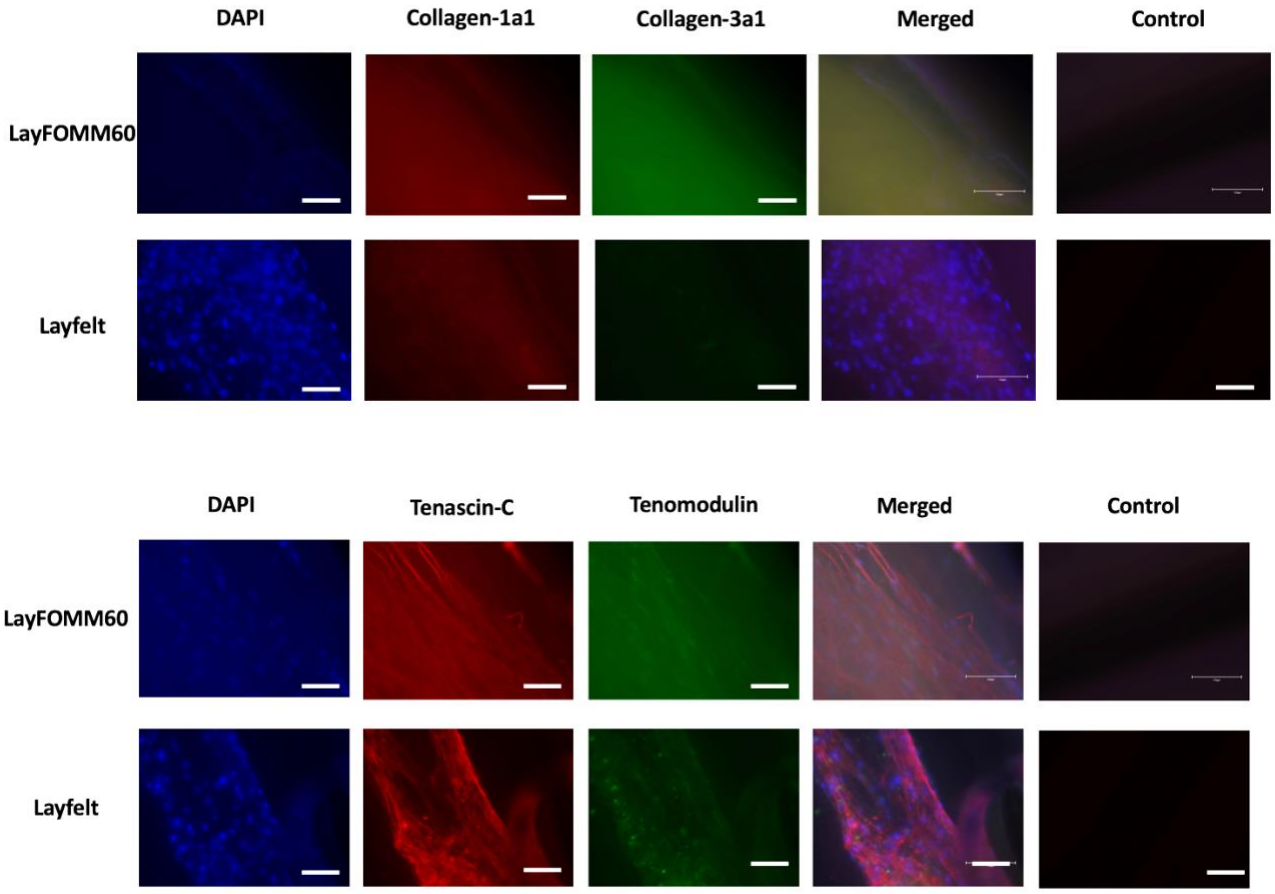

Figure 17- Representative immunofluorescence images of ASCs cultured on LayFOMM60 and Layfelt for 21 days. Enhanced signal tenogenic proteins on both the scaffolds suggest tenogenic matrix deposition on cell-seeded scaffolds after 21 days compared to the uncoated control. Scale bar = 250 μm, magnification 10X.

CHAPTER 5

DISCUSSION

Almost 30 years ago, tissue engineering emerged as a promising regenerative medicine technique. Since then, it has attracted much attention by making several advancements in the regeneration of bone, cartilage, heart, pancreas, and other organs. Low-cost 3D printed scaffolds providing shelter to host cells have revolutionized the field of neo-tissue formation. Stem cells are now being used to differentiate and repair complex connective tissues like tendons and ligaments. While many of these scaffolds and stem cells show promise, proper tissue integration and mechanical failure tend to be the primary cause of transplanted tissue failure. Therefore, there is a need to explore biomaterials and stem cell sources that can prove to be good options for regenerating viable tendon and ligament tissue substitutes. In this study, we investigated the mechanical, chemical, and biological properties of two polyurethane polymers, i.e., LayFomm60 and Layfelt and their biocompatibility with adipose stromal cells. LayFOMM60 is a polymer of interest because of its ease of forming complex and customizable scaffolds through a low-cost additive manufacturing process and its ability to reveal micro and nano porosities by simply washing the material with DI water. These porosities create surface roughness that promotes cell adhesion, proliferation, and ingrowth. Due to the porous nature of LayFOMM60, it has previously been used to deliver small molecules like growth factors to the implantation site.

Along with the advantages mentioned above, washed Layfelt has shown fiber alignment similar to the alignment of collagen fibrils shown in ACL through electron microscopy. Like LayFOMM60, Layfelt is also porous and can be easily 3D printed with intricate geometries. There are limited studies on both materials, and their potential as ligament graft substitutes are not yet explored. In

native ligament and tendon tissues, tenocytes and ligament fibroblasts are aligned between long and parallel collagen fibrils. But in *in vitro* culture of tendon and ligament fibroblasts cells, these cells do not align in rows suggesting the influence of either biomechanical forces or parallelly aligned collagen fibrils on the cell alignment [26]. Thus, in this study, we 3D printed LayFOMM60 and Layfelt scaffolds with aligned fibers in 3 different crimp patterns to mimic the topographic cues of native tendon and ligament tissue and investigated its biomechanical properties.

5.1 Constant fluid holding capacity of porous LayFOMM60 and Layfelt with minimal degradation

The human knee joint has space limited by synovium, and uncontrolled expansion of graft tissue can impede the joint space by causing its narrowing, leading to complications like arthritis. We studied the fluid holding capacity of the graft material, i.e., LayFOMM60 and Layfelt and found that the fluid holding capacity of both LayFOMM60 and Layfelt remained constant over 21 days. LayFOMM60 absorbed water equivalent to 35% of its dry weight, and Layfelt absorbed water equivalent to 45% of its dry weight. The fluid was retained over time, preventing repetitive expansion and contraction of the graft material, indicating the stability of the material.

We investigated the chemical composition of the two materials and found that Layfelt has more PVA content than LayFOMM60, hence more porous and fluid-holding capacity. These porosities help to better represent the actual *in vivo* micro-environment of the extracellular matrix that cells are exposed to [110]. Due to these porosities, an open interconnected network is formed, which helps in facilitating nutrient and oxygen diffusion and waste removal, which is essential for cell nutrition and proliferation for tissue neo-vascularization and new tissue formation [72, 110, 111, 152, 153]. It also facilitates mechanical retention of the graft by facilitating mechanical interlocking between the graft tissue and the surrounding tissue [110, 154]. These porosities also

promote crosstalk between cells by facilitating the exchange of released paracrine factors. However, these porosities may result in compromised mechanical strength.

In this study, we found that LayFOMM60 and Layfelt demonstrated minimal degradation over 90 days under *in vitro* conditions. This can result in restricted cell proliferation and deficiency of oxygen and nutrients in the regenerating tissue. Ideally, the scaffold's degradation rate should match the tissue growth rate to maintain the implant's mechanical and structural integrity before the regenerated tissue is sufficiently developed. ACL regeneration is a slow process, and its functionality requires at least six months [72]. For ACL regeneration, materials with slow degradation, like LayFOMM60 and Layfelt, should be selected. This study assessed degradation by incubating filaments in double distilled water at body temperature. However, *in vivo* degradation is faster due to tissue inflammatory response and mechanical stimulations [72]. *In vivo* degradation can also be accelerated by the secretion of enzymes like esterases from bacteria such as pseudomonas but infection in ACL reconstruction is infrequent, with rates of only 0.14-0.7%{170}.

5.2 Inferior mechanical properties of 3D printed LayFOMM60 and Layfelt scaffolds as compared to native ACL

Appropriate mechanical strength is crucial at the initial stages of graft implantation. An ideal ACL graft should have a tensile strength similar to native tissue. LayFOMM60 and Layfelt are flexible polymers with tensile properties like apparent modulus, ultimate tensile strength and % strain at failure lower than ACL. In future studies, measures to improve the tensile properties of these scaffolds need to be taken. Standard techniques for fabricating scaffolds in tissue engineering are salt leaching, gas forming, phase separation, and freeze-drying. Still, these techniques do not allow precise control over internal scaffold geometry, and the formation of complex scaffolds and their

consistent replicability using these techniques can be challenging [110, 155, 156]. Rapid prototyping technique using computer-aided design (CAD) modelling, also known as Additive Manufacturing or 3D printing, allows the use of various materials with mechanical properties ranging from soft tissue to hard tissues, with consistency and replicability [157-160]. 3D printers with multiple nozzles can be used to co-print a variety of materials to form a composite scaffold. Thus, to improve the mechanical strength of LayFOMM60 and Layfelt scaffolds, we can co-print these flexible materials with a rigid polymer like Polylactic acid (PLA), Polylactic co-glycolic acid (PLGA), and polycaprolactone (PCL).

5.3 ASCs remained viable and metabolically on LayFOMM60, Layfelt and PLA scaffolds

To study the biocompatibility of ASCs on 3D printed scaffolds, we seeded the cells on LayFOMM60, Layfelt and PLA scaffolds to study cell adhesion, cell viability and metabolic activity as cell response. We found low ASCs cell adhesion on all the scaffolds, i.e., LayFOMM60, Layfelt and PLA, although cells seeded on all the materials showed good cell viability and remained metabolically active. Attachment of cells to the 3D printed scaffold, and ability to remain viable and metabolically active after 7 days of 3D culture at body temperature, indicates biocompatibility of the cell-seeded scaffolds *in vivo* as well. One strategy to improve cell availability to the scaffold could be the pre-fabrication of scaffolds before cell seeding by encapsulating cells within the scaffold rather than seeding them on the surface. This could be accomplished using bioprinting technology—this technique 3D prints with living inks containing cells. Cell encapsulation within the scaffold will also protect the cells from the immune system. The main limitation of this technique is the transportation of oxygen and nutrients to the cells, but the inherent porosities can overcover this in washed LayFOMM60 and Layfelt materials. Like 3D printing, co-printing of various flexible and rigid polymers can be done through bioprinting to

fabricate a composite scaffold with sufficient mechanical strength to maintain integrity until new tissue regenerates.

5.4 Upregulation of SCX gene and expression of tenogenic proteins indicating deposition of T/L ECM

Studies have shown that Scleraxis is one of the earliest differentiation markers toward the tenogenic lineage [161]. In our research, SCX was upregulated on all three scaffolds indicating tenogenic differentiation after seven days of cell seeding. Protein analysis at 21 days showed the formation of a tendon matrix, with robust detection of collagen 1a1, collagen 3a1, tenomodulin and tenascin-C. Collagen type I is the most abundant component of ECM, and Collagen type III is found in tendon matrices. In addition, tenascin-C and tenomodulin are mechanoresponsive proteins that aid in tendon cell proliferation and matrix assembly. Expression of the SCX gene on day 7 signifies the initiation of differentiation of ASCs towards the tenogenic lineage, and expression of proteins on day 21 indicates the commitment of ASCs towards the tenogenic lineage. However, further studies are required to quantify the expression of tenogenic proteins. Due to the 3-dimensional structure of the scaffold and expression of the extracellular matrix, confocal microscopy needs to be done to quantify live cells and the tenogenic protein expression.

The data presented in this study suggests that mechanical cues of the polyurethane scaffolds alone can drive the tenogenic differentiation of ASCs. However, the expression of tenogenic genes needs to be studied for an extended period. LayFOMM60 and Layfelt alone do not have sufficient mechanical strength to act as ACL grafts. Hence co-printing with rigid material needs to be done to fabricate a scaffold for improved tensile properties. Although these bioprinted scaffolds were biocompatible with ASCs *in vitro,* future studies will require the implantation of the cell-seeded

scaffold in the animal model to further study *in vivo* biocompatibility. A study by Megan *et al.* demonstrated good cell viability and matrix production on *in vivo* mandibular implantation of dental pulp stem cells seeded LayFOMM60 scaffold {158}.

CHAPTER 6

CONCLUSION

In this thesis, we investigated the chemical properties of the LayFOMM60 and Layfelt material. We generated low-cost Lay-FOMM60 and Layfelt scaffolds and tested their mechanical properties, and the results were compared to native ACL tissue. Furthermore, we tested the biocompatibility of LayFOMM60, Layfelt and PLA scaffold with human adipose stromal cells *in vitro* by testing cell adhesion, viability, metabolic activity, gene expression and ligamentogenic matrix deposition. Results suggest that LayFOMM60 and Layfelt have constant fluid holding capacity and minimal degradation. Both Layfomm60 and Layfelt scaffolds had inferior mechanical properties to ACL. But both scaffolds demonstrated good cell viability, metabolic activity, upregulation of tenogenic gene and ligamentogenic matrix deposition. Thus, LayFOMM60 and Layfelt scaffolds seeded with human adipose stromal cells may be viable ACL graft substitutes and improve long-term ACL reconstruction outcomes.

APPENDIX

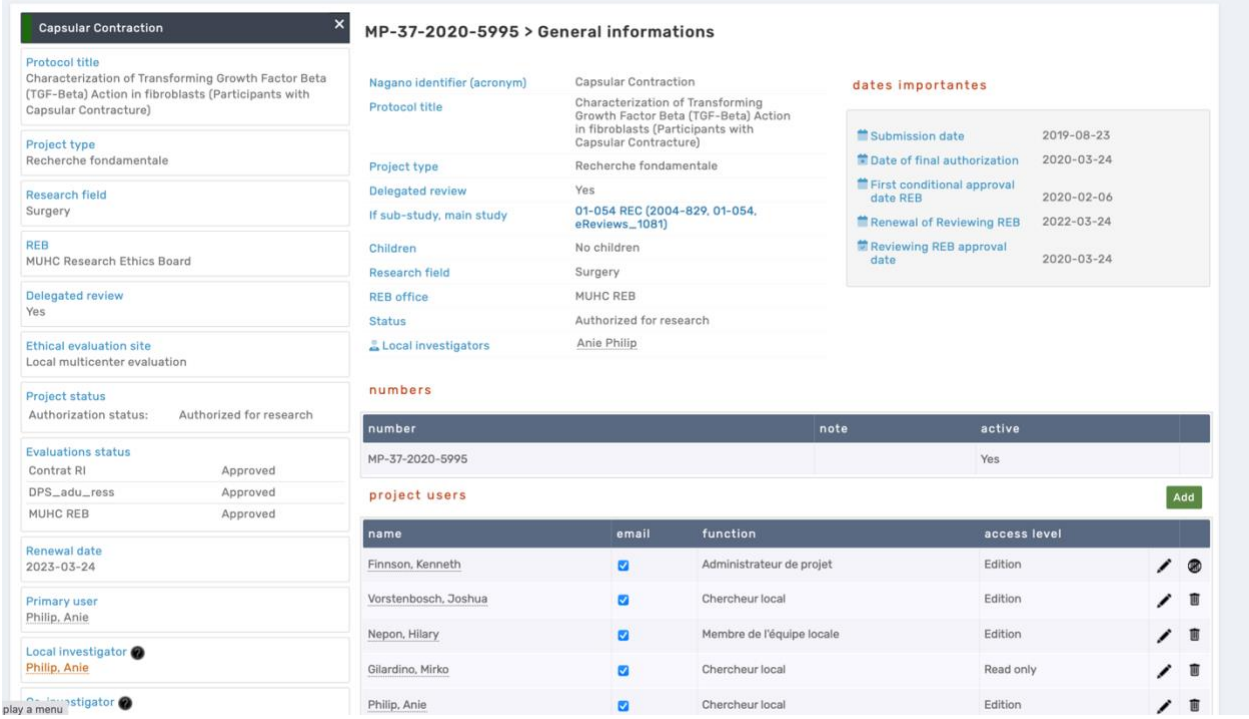

1. *REB approval for Adipose samples*

BIBLIOGRAPHY

1. Carpenter, J.E. and K.D. Hankenson, *Animal models of tendon and ligament injuries for tissue engineering applications.* Biomaterials, 2004. **25**(9): p. 1715-1722.
2. Leong, N.L., et al., *Tendon and Ligament Healing and Current Approaches to Tendon and Ligament Regeneration.* Journal of Orthopaedic Research, 2020. **38**(1): p. 7-12.
3. Yilgor, C., P. Yilgor Huri, and G. Huri, *Tissue engineering strategies in ligament regeneration.* Stem cells international, 2012. **2012**.
4. Kuo, C.K., J.E. Marturano, and R.S. Tuan, *Novel strategies in tendon and ligament tissue engineering: advanced biomaterials and regeneration motifs.* BMC sports science, medicine and rehabilitation, 2010. **2**(1): p. 1-14.
5. Rodrigues, M.T., R.L. Reis, and M.E. Gomes, *Engineering tendon and ligament tissues: present developments towards successful clinical products.* Journal of tissue engineering and regenerative medicine, 2013. **7**(9): p. 673-686.
6. Tovar, N., et al., *A comparison of degradable synthetic polymer fibers for anterior cruciate ligament reconstruction.* Journal of Biomedical Materials Research Part A: An Official Journal of The Society for Biomaterials, The Japanese Society for Biomaterials, and The Australian Society for Biomaterials and the Korean Society for Biomaterials, 2010. **93**(2): p. 738-747.
7. Santos, M.L., et al., *Biomaterials as tendon and ligament substitutes: current developments*, in *Regenerative strategies for the treatment of knee joint disabilities*. 2017, Springer. p. 349-371.

8. Petersen, W. and B. Tillmann, *Structure and vascularization of the cruciate ligaments of the human knee joint.* Anat Embryol (Berl), 1999. **200**(3): p. 325-34.

9. Subramanian, A. and T.F. Schilling, *Tendon development and musculoskeletal assembly: emerging roles for the extracellular matrix.* Development, 2015. **142**(24): p. 4191-4204.

10. Juneja, S.C. and C. Veillette, *Defects in tendon, ligament, and enthesis in response to genetic alterations in key proteoglycans and glycoproteins: a review.* Arthritis, 2013. **2013**.

11. Sugimoto, Y., et al., *Scx+/Sox9+ progenitors contribute to the establishment of the junction between cartilage and tendon/ligament.* Development, 2013. **140**(11): p. 2280-2288.

12. Tozer, S. and D. Duprez, *Tendon and ligament: development, repair and disease.* Birth Defects Research Part C: Embryo Today: Reviews, 2005. **75**(3): p. 226-236.

13. Yang, G., B.B. Rothrauff, and R.S. Tuan, *Tendon and ligament regeneration and repair: clinical relevance and developmental paradigm.* Birth defects research part C: embryo today: reviews, 2013. **99**(3): p. 203-222.

14. Benjamin, M. and J. Ralphs, *The cell and developmental biology of tendons and ligaments.* International review of cytology, 2000. **196**: p. 85-130.

15. Schweitzer, R., et al., *Analysis of the tendon cell fate using Scleraxis, a specific marker for tendons and ligaments.* 2001.

16. Screen, H.R.C., et al., *Tendon Functional Extracellular Matrix.* Journal of Orthopaedic Research, 2015. **33**(6): p. 793-799.

17. Wang, J.H., *Mechanobiology of tendon.* J Biomech, 2006. **39**(9): p. 1563-82.

18. Evans, J.H. and J.C. Barbenel, *Structural and mechanical properties of tendon related to function.* Equine Vet J, 1975. **7**(1): p. 1-8.

19. Hampson, K., et al., *Tendon tissue engineering.* Topics in tissue engineering, 2008. **4**: p. 1-21.

20. Fenwick, S.A., B.L. Hazleman, and G.P. Riley, *The vasculature and its role in the damaged and healing tendon.* Arthritis Res, 2002. **4**(4): p. 252-60.

21. Towler, D.A. and R.H. Gelberman, *The alchemy of tendon repair: a primer for the (S)mad scientist.* The Journal of clinical investigation, 2006. **116**(4): p. 863-866.

22. Fukuta, S., et al., *Identification of types II, IX and X collagens at the insertion site of the bovine achilles tendon.* Matrix Biol, 1998. **17**(1): p. 65-73.

23. Bailey, A.J. and N.D. Light, *Intermolecular cross-linking in fibrotic collagen.* Ciba Found Symp, 1985. **114**: p. 80-96.

24. Eyre, D.R., M.A. Paz, and P.M. Gallop, *Cross-linking in collagen and elastin.* Annu Rev Biochem, 1984. **53**: p. 717-48.

25. Léjard, V., et al., *Scleraxis and NFATc regulate the expression of the pro-alpha1(I) collagen gene in tendon fibroblasts.* J Biol Chem, 2007. **282**(24): p. 17665-75.

26. Schulze-Tanzil, G., et al., *Decellularized Tendon Extracellular Matrix—A Valuable Approach for Tendon Reconstruction?* Cells, 2012. **1**(4): p. 1010-1028.

27. Pins, G.D., et al., *Self-assembly of collagen fibers. Influence of fibrillar alignment and decorin on mechanical properties.* Biophys J, 1997. **73**(4): p. 2164-72.

28. Vogel, K.G. and T.J. Koob, *Structural specialization in tendons under compression.* Int Rev Cytol, 1989. **115**: p. 267-93.

29. Elefteriou, F., et al., *Binding of tenascin-X to decorin.* FEBS Letters, 2001. **495**(1): p. 44-47.

30. Bi, Y., et al., *Identification of tendon stem/progenitor cells and the role of the extracellular matrix in their niche.* Nature Medicine, 2007. **13**(10): p. 1219-1227.

31. Le Huec, J.C., et al., *Epicondylitis after treatment with fluoroquinolone antibiotics.* J Bone Joint Surg Br, 1995. **77**(2): p. 293-5.

32. Chuen, F.S., et al., *Immunohistochemical characterization of cells in adult human patellar tendons.* J Histochem Cytochem, 2004. **52**(9): p. 1151-7.

33. Goodship, A.E., H.L. Birch, and A.M. Wilson, *The pathobiology and repair of tendon and ligament injury.* Vet Clin North Am Equine Pract, 1994. **10**(2): p. 323-49.

34. Galloway, M.T., A.L. Lalley, and J.T. Shearn, *The role of mechanical loading in tendon development, maintenance, injury, and repair.* The Journal of bone and joint surgery. American volume, 2013. **95**(17): p. 1620.

35. Scott, A., et al., *Mechanical force modulates scleraxis expression in bioartificial tendons.* J Musculoskelet Neuronal Interact, 2011. **11**(2): p. 124-132.

36. Beynnon, B.D., et al., *Treatment of Anterior Cruciate Ligament Injuries, Part I.* The American Journal of Sports Medicine, 2005. **33**(10): p. 1579-1602.

37. Wilmink, J., A.M. Wilson, and A.E. Goodship, *Functional significance of the morphology and micromechanics of collagen fibers in relation to partial rupture of the superficial digital flexor tendon in racehorses.* Res Vet Sci, 1992. **53**(3): p. 354-9.

38. Hope, M. and T.S. Saxby, *Tendon healing.* Foot and ankle clinics, 2007. **12**(4): p. 553-567.

39. Carpenter, J., et al., *Rotator cuff defect healing: a biomechanical and histologic analysis in an animal model.* Journal of Shoulder and Elbow Surgery, 1998. **7**(6): p. 599-605.

40. Molloy, T., Y. Wang, and G.A.C. Murrell, *The Roles of Growth Factors in Tendon and Ligament Healing.* Sports Medicine, 2003. **33**(5): p. 381-394.

41. Bedi, A., et al., *Cytokines in rotator cuff degeneration and repair.* Journal of Shoulder and Elbow Surgery, 2012. **21**(2): p. 218-227.

42. Marui, T., et al., *Effect of growth factors on matrix synthesis by ligament fibroblasts.* Journal of Orthopaedic Research, 1997. **15**(1): p. 18-23.

43. Oshiro, W., et al., *Flexor tendon healing in the rat: a histologic and gene expression study.* The Journal of hand surgery, 2003. **28**(5): p. 814-823.

44. Trad, Z., et al., *FEM analysis of the human knee joint: a review*. 2018: Springer.

45. Vaienti, E., et al., *Understanding the human knee and its relationship to total knee replacement.* Acta Bio Medica: Atenei Parmensis, 2017. **88**(Suppl 2): p. 6.

46. Zlotnicki, J.P., et al., *Basic biomechanic principles of knee instability.* Current Reviews in Musculoskeletal Medicine, 2016. **9**(2): p. 114-122.

47. Laasanen, M., et al., *Biomechanical properties of knee articular cartilage.* Biorheology, 2003. **40**(1, 2, 3): p. 133-140.

48. Sophia Fox, A.J., A. Bedi, and S.A. Rodeo, *The Basic Science of Articular Cartilage: Structure, Composition, and Function.* Sports Health: A Multidisciplinary Approach, 2009. **1**(6): p. 461-468.

49. Cohen, N.P., R.J. Foster, and V.C. Mow, *Composition and dynamics of articular cartilage: structure, function, and maintaining healthy state.* Journal of Orthopaedic & Sports Physical Therapy, 1998. **28**(4): p. 203-215.

50. Petersen, W. and B. Tillmann, *Structure and vascularization of the cruciate ligaments of the human knee joint.* Anatomy and Embryology, 1999. **200**(3): p. 325-334.

51. Zantop, T., et al., *Anterior cruciate ligament anatomy and function relating to anatomical reconstruction.* Knee Surgery, Sports Traumatology, Arthroscopy, 2006. **14**(10): p. 982-992.

52. Duthon, V.B., et al., *Anatomy of the anterior cruciate ligament.* Knee Surgery, Sports Traumatology, Arthroscopy, 2006. **14**(3): p. 204-213.

53. Zantop, T., W. Petersen, and F.H. Fu, *Anatomy of the anterior cruciate ligament.* Operative Techniques in Orthopaedics, 2005. **15**(1): p. 20-28.

54. Markatos, K., et al., *The anatomy of the ACL and its importance in ACL reconstruction.* European Journal of Orthopaedic Surgery & Traumatology, 2013. **23**(7): p. 747-752.

55. Reiman, P. and D. Jackson, *Anatomy of the anterior cruciate ligament*, in *The anterior cruciate deficient knee*. 1987, CV Mosby St. Louis, MO. p. 17-26.

56. Petersen, W. and B. Tillmann, *Anatomy and function of the anterior cruciate ligament.* Der Orthopade, 2002. **31**(8): p. 710-718.

57. Arnoczky, S.P., *Anatomy of the anterior cruciate ligament.* Clinical orthopaedics and related research, 1983(172): p. 19-25.

58. Woo, S.L., et al., *Biomechanics and anterior cruciate ligament reconstruction.* Journal of Orthopaedic Surgery and Research, 2006. **1**(1): p. 1-9.

59. Amis, A.A. and G. Dawkins, *Functional anatomy of the anterior cruciate ligament. Fiber bundle actions related to ligament replacements and injuries.* The Journal of bone and joint surgery. British volume, 1991. **73**(2): p. 260-267.

60. KENNEDY, J.C., H.W. WEINBERG, and A.S. WILSON, *The anatomy and function of the anterior cruciate ligament: as determined by clinical and morphological studies.* JBJS, 1974. **56**(2): p. 223-235.

61. Odensten, M. and J. Gillquist, *Functional anatomy of the anterior cruciate ligament and a rationale for reconstruction.* The Journal of bone and joint surgery. American volume, 1985. **67**(2): p. 257-262.

62. Chandrashekar, N., et al., *Sex-based differences in the tensile properties of the human anterior cruciate ligament.* Journal of Biomechanics, 2006. **39**(16): p. 2943-2950.

63. Harner, C.D., et al., *Quantitative analysis of human cruciate ligament insertions.* Arthroscopy: The Journal of Arthroscopic & Related Surgery, 1999. **15**(7): p. 741-749.

64. Subit, D., et al., *Microstructure of the ligament-to-bone attachment complex in the human knee joint.* J Mech Behav Biomed Mater, 2008. **1**(4): p. 360-7.

65. Anderson, A.F., et al., *Correlation of anthropometric measurements, strength, anterior cruciate ligament size, and intercondylar notch characteristics to sex differences in anterior cruciate ligament tear rates.* The American journal of sports medicine, 2001. **29**(1): p. 58-66.

66. Girgis, F.G., J.L. Marshall, and A. Monajem, *The cruciate ligaments of the knee joint. Anatomical, functional and experimental analysis.* Clinical orthopaedics and related research, 1975(106): p. 216-231.

67. Dienst, M., R.T. Burks, and P.E. Greis, *Anatomy and biomechanics of the anterior cruciate ligament.* Orthopedic Clinics, 2002. **33**(4): p. 605-620.

68. Noyes, F.R., J.L. DeLucas, and P.J. Torvik, *Biomechanics of Anterior Cruciate Ligament Failure: An Analysis of.* J. Bone Joint Surg. Am, 1974. **56**: p. 236-253.

69. Woo, S.L.-Y., et al., *Tensile properties of the human femur-anterior cruciate ligament-tibia complex:The effects of specimen age and orientation.* The American Journal of Sports Medicine, 1991. **19**(3): p. 217-225.

70. Noyes, F.R. and E.S. Grood, *The strength of the anterior cruciate ligament in humans and Rhesus monkeys.* JBJS, 1976. **58**(8).

71. Jones, R.S., et al., *Mechanical properties of the human anterior cruciate ligament.* Clinical Biomechanics, 1995. **10**(7): p. 339-344.

72. Silva, M., et al., *Biodegradable polymer nanocomposites for ligament/tendon tissue engineering.* Journal of Nanobiotechnology, 2020. **18**(1).

73. Musahl, V. and J. Karlsson, *Anterior Cruciate Ligament Tear.* New England Journal of Medicine, 2019. **380**(24): p. 2341-2348.

74. Georgoulis, A.D., et al., *ACL injury and reconstruction: Clinical related in vivo biomechanics.* Revue de Chirurgie Orthopédique et Traumatologique, 2010. **96**(8, Supplement): p. S339-S348.

75. Ireland, M.L., *The female ACL: why is it more prone to injury?* Orthopedic Clinics of North America, 2002. **33**(4): p. 637-651.

76. Liu, S.H., et al., *Primary immunolocalization of estrogen and progesterone target cells in the human anterior cruciate ligament.* Journal of Orthopaedic Research, 1996. **14**(4): p. 526-533.

77. Hong, S.H., et al., *Grading of Anterior Cruciate Ligament Injury: Diagnostic Efficacy of Oblique Coronal Magnetic Resonance Imaging of the Knee.* Journal of Computer Assisted Tomography, 2003. **27**(5): p. 814-819.

78. Hulet, C. and et al., *The use of allograft tendons in primary ACL reconstruction.* Knee Surgery, Sports Traumatology, Arthroscopy, 2019.

79. Dashe, J., et al., *Allograft tissue irradiation and failure rate after anterior cruciate ligament reconstruction: A systematic review.* World Journal of Orthopedics, 2016. **7**(6): p. 392.

80. Arnoczky, S.P., R.F. Warren, and M.A. Ashlock, *Replacement of the anterior cruciate ligament using a patellar tendon allograft. An experimental study.* J Bone Joint Surg Am, 1986. **68**(3): p. 376-85.

81. Prodromos, C., B. Joyce, and K. Shi, *A meta-analysis of stability of autografts compared to allografts after anterior cruciate ligament reconstruction.* Knee Surg Sports Traumatol Arthrosc, 2007. **15**(7): p. 851-6.

82. Crawford, C., et al., *Investigation of postoperative allograft-associated infections in patients who underwent musculoskeletal allograft implantation.* Clin Infect Dis, 2005. **41**(2): p. 195-200.

83. Han, H.S., et al., *Anterior Cruciate Ligament Reconstruction.* Clinical Orthopaedics & Related Research, 2008. **466**(1): p. 198-204.

84. Feller, J.A., K.E. Webster, and B. Gavin, *Early post-operative morbidity following anterior cruciate ligament reconstruction: patellar tendon versus hamstring graft.* Knee Surg Sports Traumatol Arthrosc, 2001. **9**(5): p. 260-6.

85. Sachs, R.A., et al., *Patellofemoral problems after anterior cruciate ligament reconstruction.* The American Journal of Sports Medicine, 1989. **17**(6): p. 760-765.

86. Joseph, M., et al., *Short-term recovery after anterior cruciate ligament reconstruction: a prospective comparison of three autografts.* Orthopedics, 2006. **29**(3): p. 243-8.

87. Colombet, P., et al., *Anterior cruciate ligament reconstruction using four-strand semitendinosus and gracilis tendon grafts and metal interference screw fixation.* Arthroscopy, 2002. **18**(3): p. 232-7.

88. Mikkelsen, C., S. Werner, and E. Eriksson, *Closed kinetic chain alone compared to combined open and closed kinetic chain exercises for quadriceps strengthening after anterior cruciate ligament reconstruction with respect to return to sports: a prospective matched follow-up study.* Knee Surg Sports Traumatol Arthrosc, 2000. **8**(6): p. 337-42.

89. Muellner, T., et al., *Shortening of the patellar tendon after anterior cruciate ligament reconstruction.* Arthroscopy, 1998. **14**(6): p. 592-6.

90. Zeng, C., et al., *Autograft Versus Allograft in Anterior Cruciate Ligament Reconstruction: A Meta-analysis of Randomized Controlled Trials and Systematic Review of Overlapping Systematic Reviews.* Arthroscopy, 2016. **32**(1): p. 153-63.e18.

91. Marrale, J., M.C. Morrissey, and F.S. Haddad, *A literature review of autograft and allograft anterior cruciate ligament reconstruction.* Knee Surgery, Sports Traumatology, Arthroscopy, 2007. **15**(6): p. 690-704.

92. Klimkiewicz, J.J., et al., *Comparison of human tendon allografts and autografts used in knee reconstruction.* Current Orthopaedic Practice, 2011. **22**: p. 494–502.

93. McGuire, D.A. and S.D. Hendricks, *Allograft Tissue in ACL Reconstruction.* Sports Medicine and Arthroscopy Review, 2009. **17**(4): p. 224-233.

94. Potenza, A.D., *Tendon Healing Within the Flexor Digital Sheath in the Dog: An Experimental Study.* JBJS, 1962. **44**(1): p. 49-64.

95. Takasugi, H., et al., *Three-dimensional architecture of blood vessels of tendons demonstrated by corrosion casts.* Hand, 1978. **10**(1): p. 9-15.

96. Schmidt-Rohlfing, B., et al., *The blood supply of the Achilles tendon.* Int Orthop, 1992. **16**(1): p. 29-31.

97. Ahmed, I.M., et al., *Blood supply of the Achilles tendon.* J Orthop Res, 1998. **16**(5): p. 591-6.

98. Meyers, S.A., et al., *Effect of hyaluronic acid/chondroitin sulfate on healing of full-thickness tendon lacerations in rabbits.* J Orthop Res, 1989. **7**(5): p. 683-9.

99. Zuk, P.A., et al., *Multilineage cells from human adipose tissue: implications for cell-based therapies.* Tissue Eng, 2001. **7**(2): p. 211-28.

100. Mizuno, H., M. Tobita, and A.C. Uysal, *Concise review: Adipose-derived stem cells as a novel tool for future regenerative medicine.* Stem Cells, 2012. **30**(5): p. 804-10.

101. Longo, U.G., et al., *Scaffolds in Tendon Tissue Engineering.* Stem Cells International, 2012. **2012**: p. 1-8.

102. Ahangar, P., et al., *Nanoporous 3D-printed scaffolds for local doxorubicin delivery in bone metastases secondary to prostate cancer.* Materials, 2018. **11**(9): p. 1485.

103. Pitaru, A.A., et al., *Investigating Commercial Filaments for 3D Printing of Stiff and Elastic Constructs with Ligament-Like Mechanics.* Micromachines, 2020. **11**(9): p. 846.

104. Cooke, M.E., et al., *3D printed polyurethane scaffolds for the repair of bone defects.* Frontiers in Bioengineering and Biotechnology, 2020. **8**: p. 557215.

105. Pitaru, A.A., et al., *3D Printing to Microfabricate Stiff and Elastic Scaffolds that Mimic Ligament Tissue.*

106. Akoury, E., M.H. Weber, and D.H. Rosenzweig, *3D-Printed nanoporous scaffolds impregnated with zoledronate for the treatment of spinal bone metastases.* MRS Advances, 2019. **4**(21): p. 1245-1251.

107. Lacombe, J.-G., *In Vitro Tissue Engineering Strategies for Augmented ACL Reconstruction*. 2021, McGill University (Canada).

108. https://www.matterhackers.com/store/3d-printer-filament/poro-lay-lay-fomm-60-porous-filament-175mm

109. Oberoi, G., et al., *The impact of 3D-printed LAY-FOMM 40 and LAY-FOMM 60 on L929 cells and human oral fibroblasts.* Clinical Oral Investigations, 2021. **25**(4): p. 1869-1877.

110. Loh, Q.L. and C. Choong, *Three-dimensional scaffolds for tissue engineering applications: role of porosity and pore size.* 2013.

111. Hollister, S.J., *Porous scaffold design for tissue engineering.* Nature materials, 2005. **4**(7): p. 518-524.

112. Wu, C., et al., *Three-dimensional printing of hierarchical and tough mesoporous bioactive glass scaffolds with a controllable pore architecture, excellent mechanical strength and mineralization ability.* Acta biomaterialia, 2011. **7**(6): p. 2644-2650.

113. Seitz, H., et al., *Three-dimensional printing of porous ceramic scaffolds for bone tissue engineering.* Journal of Biomedical Materials Research Part B: Applied Biomaterials: An Official Journal of The Society for Biomaterials, The Japanese Society for Biomaterials, and The Australian Society for Biomaterials and the Korean Society for Biomaterials, 2005. **74**(2): p. 782-788.

114. Caddeo, S., M. Boffito, and S. Sartori, *Tissue Engineering Approaches in the Design of Healthy and Pathological In Vitro Tissue Models.* Frontiers in Bioengineering and Biotechnology, 2017. **5**.

115. Takahashi, K. and S. Yamanaka, *Induction of pluripotent stem cells from mouse embryonic and adult fibroblast cultures by defined factors.* Cell, 2006. **126**(4): p. 663-76.

116. Ben-David, U. and N. Benvenisty, *The tumorigenicity of human embryonic and induced pluripotent stem cells.* Nat Rev Cancer, 2011. **11**(4): p. 268-77.

117. Lenoir, N., *Europe confronts the embryonic stem cell research challenge.* Science, 2000. **287**(5457): p. 1425-7.

118. Oshita, T., et al., *Adipose-Derived Stem Cells Improve Collagenase-Induced Tendinopathy in a Rat Model.* The American Journal of Sports Medicine, 2016. **44**(8): p. 1983-1989.

119. Weisberg, S.P., et al., *Obesity is associated with macrophage accumulation in adipose tissue.* J Clin Invest, 2003. **112**(12): p. 1796-808.

120. Xu, H., et al., *Chronic inflammation in fat plays a crucial role in the development of obesity-related insulin resistance.* J Clin Invest, 2003. **112**(12): p. 1821-30.

121. Schipper, B.M., et al., *Regional anatomic and age effects on cell function of human adipose-derived stem cells.* Ann Plast Surg, 2008. **60**(5): p. 538-44.

122. Prunet-Marcassus, B., et al., *From heterogeneity to plasticity in adipose tissues: site-specific differences.* Exp Cell Res, 2006. **312**(6): p. 727-36.

123. Seale, P., et al., *PRDM16 controls a brown fat/skeletal muscle switch.* Nature, 2008. **454**(7207): p. 961-7.

124. Jeon, B.G., et al., *Characterization and comparison of telomere length, telomerase and reverse transcriptase activity and gene expression in human mesenchymal stem cells and cancer cells of various origins.* Cell Tissue Res, 2011. **345**(1): p. 149-61.

125. Kim, W.S., B.S. Park, and J.H. Sung, *Protective role of adipose-derived stem cells and their soluble factors in photoaging.* Arch Dermatol Res, 2009. **301**(5): p. 329-36.

126. Rehman, J., et al., *Secretion of angiogenic and antiapoptotic factors by human adipose stromal cells.* Circulation, 2004. **109**(10): p. 1292-8.

127. Salgado, A.J., et al., *Adipose tissue derived stem cells secretome: soluble factors and their roles in regenerative medicine.* Curr Stem Cell Res Ther, 2010. **5**(2): p. 103-10.

128. Kilroy, G.E., et al., *Cytokine profile of human adipose-derived stem cells: expression of angiogenic, hematopoietic, and pro-inflammatory factors.* J Cell Physiol, 2007. **212**(3): p. 702-9.

129. *Unknown article.*

130. Chen, C.H., et al., *Response of Dermal Fibroblasts to Biochemical and Physical Cues in Aligned Polycaprolactone/Silk Fibroin Nanofiber Scaffolds for Application in Tendon Tissue Engineering.* Nanomaterials (Basel), 2017. **7**(8).

131. Yin, Z., et al., *The regulation of tendon stem cell differentiation by the alignment of nanofibers.* Biomaterials, 2010. **31**(8): p. 2163-75.

132. Orr, S.B., et al., *Aligned multilayered electrospun scaffolds for rotator cuff tendon tissue engineering.* Acta Biomater, 2015. **24**: p. 117-26.

133. Docheva, D., et al., *Biologics for tendon repair.* Advanced drug delivery reviews, 2015. **84**: p. 222-239.

134. Wang, W., et al., *Aligned nanofibers direct human dermal fibroblasts to tenogenic phenotype in vitro and enhance tendon regeneration in vivo.* Nanomedicine, 2016. **11**(9): p. 1055-1072.

135. Yin, Z., et al., *Electrospun scaffolds for multiple tissues regeneration in vivo through topography dependent induction of lineage specific differentiation.* Biomaterials, 2015. **44**: p. 173-185.

136. Zhang, C., et al., *Well-aligned chitosan-based ultrafine fibers committed teno-lineage differentiation of human induced pluripotent stem cells for Achilles tendon regeneration.* Biomaterials, 2015. **53**: p. 716-730.

137. Hakimi, O., et al., *A layered electrospun and woven surgical scaffold to enhance endogenous tendon repair.* Acta biomaterialia, 2015. **26**: p. 124-135.

138. Zheng, Z., et al., *Alignment of collagen fiber in knitted silk scaffold for functional massive rotator cuff repair.* Acta biomaterialia, 2017. **51**: p. 317-329.

139. Chen, C.-H., et al., *Response of dermal fibroblasts to biochemical and physical cues in aligned polycaprolactone/silk fibroin nanofiber scaffolds for application in tendon tissue engineering.* Nanomaterials, 2017. **7**(8): p. 219.

140. Yin, Z., et al., *The regulation of tendon stem cell differentiation by the alignment of nanofibers.* Biomaterials, 2010. **31**(8): p. 2163-2175.

141. Orr, S.B., et al., *Aligned multilayered electrospun scaffolds for rotator cuff tendon tissue engineering.* Acta biomaterialia, 2015. **24**: p. 117-126.

142. Shi, Y., et al., *Microgrooved topographical surface directs tenogenic lineage specific differentiation of mouse tendon derived stem cells.* Biomedical Materials, 2017. **12**(1): p. 015013.

143. Teh, T.K., S.-L. Toh, and J.C. Goh, *Aligned hybrid silk scaffold for enhanced differentiation of mesenchymal stem cells into ligament fibroblasts.* Tissue Engineering Part C: Methods, 2011. **17**(6): p. 687-703.

144. Caves, J.M., et al., *Microcrimped collagen fiber-elastin composites*. Advanced Materials, 2010. **22**(18): p. 2041-2044.

145. Surrao, D.C., et al., *Self-crimping, biodegradable, electrospun polymer microfibers.* Biomacromolecules, 2010. **11**(12): p. 3624-3629.

146. Surrao, D.C., S.D. Waldman, and B.G. Amsden, *Biomimetic poly (lactide) based fibrous scaffolds for ligament tissue engineering.* Acta Biomaterialia, 2012. **8**(11): p. 3997-4006.

147. Surrao, D.C., et al., *A crimp-like microarchitecture improves tissue production in fibrous ligament scaffolds in response to mechanical stimuli.* Acta biomaterialia, 2012. **8**(10): p. 3704-3713.

148. Chao, P.-h.G., H.-Y. Hsu, and H.-Y. Tseng, *Electrospun microcrimped fibers with nonlinear mechanical properties enhance ligament fibroblast phenotype.* Biofabrication, 2014. **6**(3): p. 035008.

149. Liu, W., et al., *Generation of electrospun nanofibers with controllable degrees of crimping through a simple, plasticizer-based treatment.* Advanced materials, 2015. **27**(16): p. 2583-2588.

150. Gilbert SF. Developmental Biology. 6th edition. Sunderland (MA): Sinauer Associates; 2000. Paracrine Factors. Available from: https://www.ncbi.nlm.nih.gov/books/NBK10071/

151. Su, N., et al., *Fibrous scaffolds potentiate the paracrine function of mesenchymal stem cells: A new dimension in cell-material interaction.* Biomaterials, 2017. **141**: p. 74-85.

152. Salerno, A., et al., *Tailoring the pore structure of PCL scaffolds for tissue engineering prepared via gas foaming of multi-phase blends.* Journal of Porous Materials, 2012. **19**(2): p. 181-188.

153. Causa, F., P.A. Netti, and L. Ambrosio, *A multi-functional scaffold for tissue regeneration: the need to engineer a tissue analogue.* Biomaterials, 2007. **28**(34): p. 5093-5099.

154. Kaplan, D. and V. Karageorgiou, *Porosity of 3D biomaterial scaffolds and osteogenesis.* Biomaterials, 2005. **26**(27): p. 5474-5491.

155. Tsang, V.L. and S.N. Bhatia, *Three-dimensional tissue fabrication.* Advanced drug delivery reviews, 2004. **56**(11): p. 1635-1647.

156. Yeong, W.-Y., et al., *Rapid prototyping in tissue engineering: challenges and potential.* TRENDS in Biotechnology, 2004. **22**(12): p. 643-652.

157. Chu, T.-M.G., et al., *Mechanical and in vivo performance of hydroxyapatite implants with controlled architectures.* Biomaterials, 2002. **23**(5): p. 1283-1293.

158. Sherwood, J.K., et al., *A three-dimensional osteochondral composite scaffold for articular cartilage repair.* Biomaterials, 2002. **23**(24): p. 4739-4751.

159. Leong, K., et al., *Engineering functionally graded tissue engineering scaffolds.* Journal of the mechanical behavior of biomedical materials, 2008. **1**(2): p. 140-152.

160. Leong, K., C. Cheah, and C. Chua, *Solid freeform fabrication of three-dimensional scaffolds for engineering replacement tissues and organs.* Biomaterials, 2003. **24**(13): p. 2363-2378.

161. *Scleraxis-Overexpressed Human Embryonic Stem Cell–Derived Mesenchymal Stem Cells for Tendon Tissue Engineering with Knitted Silk-Collagen Scaffold.* Tissue Engineering Part A, 2014. **20**(11-12): p. 1583-1592.